21.

Meteorological Model Based Wind Resource Assessment in the Vicinity of Block Island

Malcolm L. Spaulding[1], Marty Bell[2], Jay Titlow[3], Lauren Decker[4], Annette Grilli[1], Ravi Sharma[1], Alexander Crosby[1], and Daniel Mendelsohn[4]

[1] Ocean Engineering
University of Rhode Island
Narragansett, RI

[2]Metlogic
212 West Mountain Avenue
Fort Collins, CO 80521

[3]WeatherFlow
790 Poquoson Ave
Poquoson, VA 23662

[4]Applied Science Associates
55 Village Square
South County Commons
South Kingstown, RI 02879

Executive Summary

Hindcast simulations of the winds in the vicinity of Block Island were performed using the Regional Atmospheric Modeling System, RAMS, V6., from October 1, 2009 to February 28, 2010 to assist in evaluating various sites south of Block Island for a small wind farm. This period was selected since wind and air temperature observations were available from an offshore buoy (4 m elevation) immediately south (4.5 km) of the island and from a meteorological tower (9.9, 32, 47.6 and 57.4 m elevations) near the center, west coast of the island. The model was implemented in a four level nested system with grid resolutions of 12, 6, 2, and 0.5 km. The model was driven by NAM 12 km analyses. The model employed a 20 m vertical grid resolution at the surface, that geometrically increased with elevation. Island land cover and topography and sea surface temperature were provided by national digital data bases.

The winds during this period were predominantly from the NW, with the next most frequent direction from the NE. The wind distribution is typical of winter winds in the area, but with enhanced winds from the NE. The meteorological tower observations showed very low shear coefficients, 0.7 to 0.9, during the simulation period, typical of neutral to unstable, winter winds.

Model simulations were compared to meteorological tower observations at 57 m on shore of Block Island and showed good agreement with the data, with similar trends for passing weather events. The observed mean speed was 9.73 m/sec and the RAMS predicted was 9.3 m/sec (5.1% difference). The wind power followed a similar trend, 1000 kW/m^2 observed and 838 kW/m^2 RAMS (16.2% difference). The model predicted shear was higher than meteorological tower observations. The predicted shear coefficients increased dramatically over the island, reaching values as high as 0.45 over the southern end of the island where vegetative cover is dense. Model predictions also show lee effects from the topography/land cover at the southern end of the island (mean elevation of 35 m) for the two predominant wind directions. Lee effects were clearly noted 8 km from the island. Model predictions were also compared to winds (10 m elevation) from an offshore buoy and again showed good agreement (observed - 8.54 m/sec vs RAMS- 8.32 m/sec).

Simulations were performed for the dominant NW wind case to assess the sensitivity of the model to how the island was represented: by both its topography and land cover, or by each separately. The model predictions showed that either topography or land cover contributed substantially to lee effects.

Model predictions were integrated over the simulation period to estimate mean wind speeds and average power at 80 m. The mean wind speed and power contour lines are parallel to the RI shoreline. Wind speeds decrease from 10.2 m/sec south of Block Island to 9.7 m/sec at the northern end of the island. Power decreases from 1150 kW/m^2 to 965 kW/m^2 over the same distance. Power estimates were made at three potential locations for a small wind farm (5 to 8 turbines), SE, S and SW of the island following the state water boundary line (5 km) from the island. Mean powers were predicted to be SE- 1097 kW/m^2, S - 1139 kW/m^2, and SW -1076 kW/m^2. The S site has the highest power production potential; 3.6 to 5.4 % higher than the other two sites. The difference between the sites is due to lee effects from the island for NW winds at the SE site and for NE winds at the SW site. The SW site, in addition, is in the lee of eastern end of Long Island (Montauk Point) for westerly winds. Lee effects at the S site are minimal since winds from the N are rare. Simulations have not been performed for spring and summer months

where SW winds dominant. Winds from this direction are likely to be comparable at all three sites, since there is no lee effect and the locations are quite close. There is some degradation of winds from the W due however to lee effects from Long Island and an increase to the SW of the island due to channel enhancements for southerly winds.

Simulations, using a template based method, were performed using the observed wind rose at the AWS Met site and model predicted wind fields for eight compass directions. Predicted mean wind speeds and power densities were in generally good agreement with the hindcasts. The differences could be explained in part by the model predicting lower frequency for the NW winds and higher frequency for W winds than observed. When the model predicted wind rose at the AWS Met was used the predictive performance improved measurably.

Table of Contents

List of Figures

List of Appendices

Appendix A Titlow, J, 2010. Comparison of RAMS Model Predictions with Observations for the October 2009 to February 2010 Hindcast Period, WeatherFlow Inc., Poquoson, VA.

Appendix B Comparison of WeatherFlow Simulations and Observations at AWS Meteorological Tower on Block Island, Ocean Engineering, University of RI, Narragansett, RI.

Abstract

Hindcast simulations of the winds in the vicinity of Block Island were performed using the Regional Atmospheric Modeling System, RAMS, V6., from October 1, 2009 to February 28, 2010 to assist in evaluating various sites south of Block Island for a small wind farm. This period was selected since wind and air temperature observations were available from an offshore buoy (4 m elevation) immediately south (4.5 km) of the island and from a meteorological tower (9.9, 32, 47.6 and 57.4 m elevations) near the center, west coast of the island. The model was implemented in a four level nested system with grid resolutions of 12, 6, 2, and 0.5 km. The model was driven by NAM 12 km analyses. The model employed a 20 m vertical grid resolution at the surface, that geometrically increased with elevation. Island land cover and topography and sea surface temperature were provided by national digital data bases.

The winds during this period were predominantly from the NW, with the next most frequent direction from the NE. The wind distribution is typical of winter winds in the area, but with enhanced winds from the NE. The meteorological tower observations showed very low shear coefficients, 0.7 to 0.9, during the simulation period, typical of neutral to unstable, winter winds.

Model simulations were compared to meteorological tower observations at 57 m on shore of Block Island and showed good agreement with the data, with similar trends for passing weather events. The observed mean speed was 9.73 m/sec and the RAMS predicted was 9.3 m/sec (5.1% difference). The wind power followed a similar trend, 1000 kW/m^2 observed and 838 kW/m^2 RAMS (16.2% difference). The model predicted shear was higher than meteorological tower observations. The predicted shear coefficients increased dramatically over the island, reaching values as high as 0.45 over the southern end of the island where vegetative cover is dense. Model predictions also show lee effects from the topography/land cover at the southern end of the island (mean elevation of 35 m) for the two predominant wind directions. Lee effects were clearly noted 8 km from the island. Model predictions were also compared to winds (10 m elevation) from an offshore buoy and again showed good agreement (observed - 8.54 m/sec vs RAMS- 8.32 m/sec).

Simulations were performed for the dominant NW wind case to assess the sensitivity of the model to how the island was represented: by both its topography and land cover, or by each separately. The model predictions showed that either topography or land cover contributed substantially to lee effects.

Model predictions were integrated over the simulation period to estimate mean wind speeds and average power at 80 m. The mean wind speed and power contour lines are parallel to the RI shoreline. Wind speeds decrease from 10.2 m/sec south of Block Island to 9.7 m/sec at the northern end of the island. Power decreases from 1150 kW/m^2 to 965 kW/m^2 over the same distance. Power estimates were made at three potential locations for a small wind farm (5 to 8 turbines), SE, S and SW of the island following the state water boundary line (5 km) from the island. Mean powers were predicted to be SE- 1097 kW/m^2, S - 1139 kW/m^2, and SW -1076 kW/m^2. The S site has the highest power production potential; 3.6 to 5.4 % higher than the other two sites. The difference between the sites is due to lee effects from the island for NW winds at the SE site and for NE winds at the SW site. The SW site, in addition, is in the lee of eastern end of Long Island (Montauk Point) for westerly winds. Lee effects at the S site are minimal since winds from the N are rare. Simulations have not been performed for spring and summer months

where SW winds dominant. Winds from this direction are likely to be comparable at all three sites, since there is no lee effect and the locations are quite close. There is some degradation of winds from the W due however to lee effects from Long Island and an increase to the SW of the island due to channel enhancements for southerly winds.

Simulations, using a template based method, were performed using the observed wind rose at the AWS Met site and model predicted wind fields for eight compass directions. Predicted mean wind speeds and power densities were in generally good agreement with the hindcasts. The differences could be explained in part by the model predicting lower frequency for the NW winds and higher frequency for W winds than observed. When the model predicted wind rose at the AWS Met was used the predictive performance improved measurably.

1. Introduction

The RI Ocean Special Area Management Plan (SAMP) has identified a potential renewable energy zone in state waters south of Block Island (Figure 1 and 2). Pear shaped, Block Island is approximately 9 km (N-S) by 6 km (widest at southern end, E-W) and was formed as an end moraine deposit from the most recent glacial ice sheet advance. The southern end of the island has a mean elevation of about 35 m (Figure 3) and is characterized by rolling hills, scrub and brush cover, and pockets of deciduous trees (Figure 4). The island is located about 15 km south of the southern RI coastal line and 23 km east northeast of Montauk Point, NY. This site was selected based on a comprehensive screening analysis and the application of a Technology Development Index (TDI) that evaluates the technical challenge to siting of lattice jacket supported wind turbines to the available power at the site (Spaulding et al, 2010a; Grilli et al, 2010). It was also identified in ATM's (2007a, b) initial screening study for offshore wind development. The analysis was performed on a 50 m spatial grid and included consideration of water depth, wind resources, cost of lattice jacket structures, and the construction effort for a pile foundation system. After consideration for marine traffic, and the impacts on marine fisheries, birds and marine mammals, a 2 km wide arc extending from SSW to E of the southern end of Block Island was selected (Figure 2). The seaward edge of the zone is bounded either by the state water boundary or the designated navigation precautionary area to the east.

One concern in the siting was the impact of topography and associated land cover on the wind resources in the immediate vicinity of the island, particularly for winds from the NW and NE, which are predominant in the winter. The concern was that the turbines would be adversely impacted by the lee effects of the island. Grilli et al's (2010) study addressed this issue by evaluating the sensitivity of predictions to two different wind resource estimates; one based on a coarse (2.5 km) grid meteorological model simulation product provided by Brower (2007) and the second based on a template scaling method using meteorological model predictions for eight compass directions and then scaling these estimates using an annual wind rose (Spaulding et al, 2010b). The two methods give substantially different results, with the later method showing more pronounced lee effects to the SE of the island.

The goal of the present study is to determine how the power production potential varies within the proposed renewable energy zone, during a winter period, when NW and NE winds dominate and the lee effects to the south of the island are expected to be important. To accomplish this goal, a four level nested version of the RAMs meteorological system is applied to predict the three dimensional wind, temperature, and pressure field in the vicinity of the island

from October 1, 2009 to February 28, 2010. Wind data is available from an offshore buoy 5 km south of Block Island and from a meteorological tower located on the western coast, about mid island during this period. Model predictions are next validated with the observations. Finally wind power estimates are made for the renewable energy zone shown in Figure 2. Section 2 presents an overview of the observation data available and Section 3 a summary of the RAMS meteorological modeling system and its application to the study area. Selected model predictions for typical NW and NE winds are provided in Section 4. Section 5 presents a comparison of model predictions to observation and 6 summarizes the power estimates for the renewable energy zones. Conclusions are presented in Section 7.

2. Observations

Two data sets are available for model validation for the simulation period from October 1, 2009 through February 28, 2010. They are summarized below:

Ocean SAMP Buoy MDS02 (Lat: 41.1, Long: 41.56)(MDS)

The University of Maine, on behalf of the Ocean SAMP study, deployed an offshore buoy with meteorological and oceanographic sensors immediately south of Block Island at the state water boundary line. The buoy collects wind speed and direction and air and sea surface temperature data every 15 minutes. The data is distributed through the Northeast Regional Association of Coastal Ocean Observing Systems web site (www.neracoos.org). The buoy has been in operation from Oct 1, 2009 to present.

AWS True Winds Block Island Meteorological Tower (AWS Met) (Lat: 41°11'49.96"N, Long: 71°35'30.34"W)

AWS True Winds erected a meteorological tower at the western entrance to Great Salt Pond. Wind speed and direction data are being collected at elevations of 9.9, 32, 47.6, and 57.4 m. Data is available from Aug 2009 to present.

Additional data sets are available in the area from Army Corp WIS study (WIS101, hindcast, 1980-1999), Department of Energy Site (DOE, 1977-1981), Block Island Airport (KBID, 1997 to 2009), and WeatherFlow's site at Block Island Jetty (2005 to 2009). They are of secondary interest for the present study. Spaulding et al (2010b) discuss these data sets in detail.

Figure 5 and 6 show the wind frequency and power roses, respectively for MDS and AWS Met stations. Data for the other stations are shown for reference but are not discussed in depth since they represent annual estimates and were collected outside the simulation period. The observations at MDS are at a 4 m elevation and those at AWS Met are at 9.9 m. During the winter observation period, both wind frequency and power roses are dominated by NW winds, followed by NE winds. Figure 7 shows the average wind power density by direction, consistent with Figure 6, the power is dominated by NW winds. Wind and power roses were analyzed for additional elevations at AWS Met and showed a similar structure. Values are shown at 32 and 57 m in Figures 7 and 8, respectively. The figures also show Weibull distribution fits to the data. The shape parameter, k, is typically in the range of 2.15 to 2.21. The amplitude parameter, c, increases with elevation from 4.62 at 10 m, to 9.66 at 32 m, to 10.12 at 57 m. Over the period of interest the wind shear coefficients at this site were typically in the range of 0.06 to 0.09, indicating a neutral to unstable boundary layer and well mixed conditions. Buoy observations

show that the air temperature was colder than the water temperature during most of this period, consistent with an unstable atmosphere.

3. High Resolution Meteorological Modeling in Study Area

RAMS, the Regional Atmospheric Modeling System (Piekle et al, 1992; Walko et al, 2000; and Tremback and Walko, 2010), is a highly versatile numerical code developed by several groups over the years, including the scientists at Colorado State University, the *ASTER division of Mission Research Corporation, and ATMET. RAMS is used for simulating and forecasting meteorological phenomena and for depicting the results. A detailed description of RAMS can be found at http://rams.atmos.colostate.edu/rams-description.html. Applications of RAMS to siting of wind energy facilities offshore and in varying terrain are presented in Alessandria et al (2009), Castellini et al (200), Guenard et al (2008), and Sukegawa et al (2006).

RAMS is primarily a limited area model, and many of its parameterizations have been designed for mesoscale or higher resolution scale grids. There is no lower limit to the domain size or to the mesh cell size of the model's finite difference grid; microscale phenomena such as tornadoes and boundary layer eddies, as well as sub-microscale turbulent flow over buildings and in a wind tunnel, have been simulated with this code. Two-way interactive grid nesting in RAMS allows local fine mesh grids to resolve small-scale atmospheric systems such as thunderstorms, while simultaneously modeling the large-scale environment of the systems on a coarser grid.

The atmospheric model is constructed around the full set of non-hydrostatic, compressible equations that atmospheric dynamics and thermodynamics, plus conservation equations for scalar quantities such as water vapor and liquid and ice hydrometeor mixing ratios. These equations are supplemented with a large selection of parameterizations for turbulent diffusion, solar and terrestrial radiation, moist processes including the formation and interaction of clouds and precipitating liquid and ice hydrometeors, kinematic effects of terrain, cumulus convection, and sensible and latent heat exchange between the atmosphere and the surface, which consists of multiple soil layers, vegetation, snow cover, canopy air, and surface water.

For the present study daily simulations starting at 0Z were performed with RAMS version 6.1. The model employed a 500 m horizontal grid spacing on the high resolution grid telescopically nested from 12 km, 6 km and 2 km grids (Figure 10 and 11). A range of horizontal grid resolutions from 4 km to 250 m were tested. In most cases, the convergence of results at the proposed turbine locations occurred at 1-2 km. In some cases, where stable conditions existed and the proposed wind farm sites were downwind of the island, differences were apparent down to 500 m. 20 m vertical grid spacing, expanding upward with a geometric ratio of 1.15 was employed. Vertical grid resolutions from 40 m to 5 m were evaluated. Testing showed a loss in wind speed of up to 5 % when the vertical resolution was lowered from 5 to 20 m. 20 m was used in this study in order to complete the 5 months of hindcasting in a timely fashion.

RAMS was initialized 6 hours prior to the 0Z start time (tau 0), firstly with a 2 grid run (outer grids only) from tau -6 to tau -3 (stage 1), then with all 4 grids from tau -3 to tau 0 (stage 2). Simulations were initialized from the 12km NAM analysis, with grid 1 bounded by subsequent 6 hourly 12 km National Center for Environmental Prediction (NCEP) North America Meteorology Model (NAM) analyses. In stage 1, the wind speed and direction, pressure, and air temperature model fields in the interior domain were strongly nudged to the

interpolated NAM analysis values. In stage 2, the same variables were nudged, but far less strongly. The atmospheric moisture data was excluded from the nudging. This forces a balance to develop for the mechanical quantities between the model and the NAM analysis, while allowing moisture quantities (clouds and precipitation) to evolve.

The 3D (spatial and depth) soil moisture field was extracted from the 12 km NAM analysis files and interpolated to the RAMS grids and soil levels. The 2D (spatial) snow cover field was also extracted from the 12km NAM analysis files and interpolated to the RAMS grids. Sea surface temperature data was obtained from Operational Sea Surface Temperature and Sea Ice Analysis (OSTIA) which uses satellite data provided by the GHRSST project, together with in-situ observations to determine the sea surface temperature. The analysis is performed using a variant of optimal interpolation (OI) technique. The analysis is produced daily at a resolution of 1/20 degree, (approx. 5km).

Digital elevation data for the study area, including Block Island, was provided from ASTER GDEM which has a 30 m grid resolution and is referenced to the WGS84/EGM96 geoid. Surface roughness, which is a significant factor in this study, is formulated as a function of wind speed over water. Over land, contributions to the surface roughness come from the water bodies, soil, vegetative cover and topographical drag within the grid cell. RAMS partitions the land use effects into contributing patches, whose weighting on the grid scale is proportional the relative dominance of the water and vegetation cover from the MRLC land use dataset.

4. Selected Simulation Results

RAMS was used to perform high resolution simulations for the study period from October 1, 2009 through February 28, 2010. This period was selected since wind data from both the meteorological tower on Block Island (AWS Met) and the MDS buoy were available. To provide a sense of the results, model predicted winds for cases of the two predominant directions observed during the study period are provided. Figure 12a and b show wind fields for NE winds, October 29, 2009, for grids 3 and 4 (Figure 9), respectively. Figures 13a and b show similar model predictions for NW winds, January 4, 2010. Predictions are at 80 m consistent with the hub height of 3.5 MW turbines. Each case is discussed separately below.

NE, October 29, 2009

The basic pattern shows that the wind speeds increase with distance offshore from the RI coastline, with the speed contours parallel to the shoreline. This is consistent with Wengsong et al (2010) 2-d simulations of winds blowing offshore/onshore. There is clear evidence of lower speed winds to the SW of the Block Island as a result of lee effects from the southern end of the island. These effects extend at least 8 km from the island.

NW, January 4, 2010

This basic pattern for the NW case is very similar to the NE example, wind speeds increasing with distance from the coast and lee effects to the SE of Block Island. The spatial extent is similar to that for the NE case. For this case, lee effects are also noted from the topography on the northern end of the island. The impact from the northern end of the island is much reduced compared to the southern end because of the more limited area and lower elevation (Figure 3).

Simulations were performed to assess the sensitivity of the model predictions to the representation of Block Island used as input to RAMS. Model predictions were performed for December 6, 2010, a NW wind case, where the impact of both topography and land cover were considered, and where land cover and topography were modeled separately. Figure 14 shows model predictions of the wind at 80 m for the three cases: topography and roughness (upper panel), roughness only (center panel), and topography only (lower panel). The patterns for the three cases are very similar. There are differences, but these are a matter of detail. An interesting observation is that either roughness or topography can result in significant lee effects. This has important implications in that westerly winds flowing over Long Island, which has a relatively low topographic relief, can result in a significant impacted area in its lee.

Simulations performed by Freedman and Markus(2010) for the Block Island area for NW winds on December 22, 2008 and February 23, 2009 show similar patterns with those presented here.

5. Comparison of Model Predictions to Observations

Model predictions were compared to wind observations at the 57 m elevation at the AWS Met for the simulation period. Figure 15, 16, and 17 show observed and model values vs time (upper panel) and differences between the two (lower panel) for wind speed, power density, and shear coefficient, respectively. Additional details are provided in Appendix A.

The model does well in representing the passage of weather events and the associated temporal variations in wind speeds (Figure 15). The mean speeds predicted by the model are 9.23 m/sec and for the observations 9.73 m/sec; a 5.1% under prediction. The model predicted wind power density (Figure 16) is very similar in temporal structure to the observed values. Over the simulation period the model under predicts the observed value (Observed: 1000 kW/m^2 versus RAMS: 838 kW/m^2 or a difference of 16.2 %). This difference is consistent with the speed under prediction.

Cross correlations (Appendix B) were performed using observed and hindcast data at 32 and 57 m and showed high values – 0.90 or greater. Power spectral densities and coherence analysis were performed and showed high coherences (0.9) for periods of 3 days or longer. The one day coherence values decreased to 0.6. A wind power density directional analysis was performed and showed the winds from the model are slightly more westerly than those observed.

The observed and predicted shear (57.4 m vs 32.1 m) (upper panel)(differences between wind speeds at the two elevations) and differences (lower panel) vs time are provided in Figure 17. The model shows similar temporal trends to the data but the mean model predicted value (0.026) is considerably higher than the observed (0.014). The comparative mean shear coefficients are 0.08 for the observations and 0.16 for the model.

A comparison of model predicted and observed wind speed versus time at MDS, 10 m elevation, is provided in Figure 18. The model does a very good job of predicting the temporal pattern and mean winds: model mean of 8.23 m/sec compared to 8.54 m/sec for the observed or an average difference of 0.49 m/sec (5.7 %). The model predictive performance is comparable to that at AWS Met.

6. Mean Wind Speed and Power Estimates

Model predicted wind speeds were averaged at 10 and 80 m elevations over the simulation period and are shown in Figure 19. The patterns are very similar at both elevations, shore parallel contours with speeds increasing with distance offshore. Winds at 80 m are approximately 25% stronger than at 10 m. The wind speed contours are distorted (bulge) immediately south of Block Island, predominantly to the SE and SW. The former due to lee effects from NW winds and the later from similar effects from NE winds.

Model predicted average wind power and cumulative wind power are shown at 10 and 80 m elevations in Figure 20 and 21, respectively. The patterns are of course identical to those in Figure 19. The magnitudes however scale as the cube of the wind speed.

Model predicted average shear coefficients are shown in Figure 22. These are determined based on model predictions from the surface to 80 m. Shear coefficients are typically 0.105 in the area around Block Island but increase dramatically over island. They reach values of 0.4 to 0.45 on the southern end of the island. It is noted that the area to the west of the Block Island Airport has the highest shear coefficients on the island. These high shear values are consistent with the land cover distribution (Figure 4).

Model predicted time series of wind power density are provided in Figure 23 for the sites noted in Figure 10. These include a ring of sites from E to S to W, following the state water boundary line and at key observation stations (AWS Met, MDS, KBID, and WeatherFlow's BIock Island Jetty). The wind power varies dramatically over time scales of hours as a result of changing weather patterns. There are about 25 events where the wind power exceeds 4 kW/m^2. NW wind events are typically strong and sustained for several days

The values in Figure 23 were averaged over the simulation period and are shown in Figure 24. The state water boundary sites represent potential locations for a small wind farm. The values range from 1060 to 1146 kW/m^2. Power density was highest to the south of the island and lower toward the E and W. Power estimates were made at three potential locations for a small wind farm (5 to 8 turbines), SE (incorporates E, ESE, SE), S (SSE, S, SSW) and SW (SW,WSW,W) of the island following the state water boundary line (5 km) from the island. Mean powers were predicted to be SE- 1097 kW/m^2, S - 1138 kW/m^2, and SW -1076 kW/m^2. The S site has the highest power production potential; 3.6 to 5.4 % higher than the other two sites. The difference between the sites is due to lee effects from the island for NW winds at the SE site and for NE winds at the SW site. The SW site, in addition, is in the lee of the eastern end of Long Island (Montauk Point) for westerly winds. Lee effects at the S site are minimal since winds from the N are rare. Winds are also enhanced at the S site by the channeling effect of Long Island for winds from the W to SW.

The SW location has been partially eliminated based on the TDI analysis (Grilli et al, 2010) due to substantially higher construct effort to install a pile foundation in the glacial end moraine sediments. Of the two remaining sites, the S site has a marginally higher power production potential. It should be noted that this analysis has not considered winds from other times of the year. During the remainder of the year winds are observed to be predominantly from the SW. With SW winds all three locations are anticipated to experience about the same winds and hence power production potential. The simulation period under investigation covers only 5 months (October through February) and does not incorporate the spring and fall season when SW winds

are dominant. An evaluation of the data at WIS 101 shows that this represents 77% of the total energy for the year.

Spaulding et al (2010b), in a companion paper, have estimated the average wind speeds and power density for the study area using a template based scaling method. In this approach model simulations are performed for representative wind events from each point of the compass and the results weighted by a wind rose used to estimate the mean conditions. The template method was applied to the present hindcast period using the wind rose at AWS Met. The individual simulation cases were taken from 2008 and 2009 and hence are completely independent of the present hindcast period.

Figure 25 shows the template (upper panel), hindcast (center panel), and difference between the two (lower panel) for the mean wind speeds (left) and power (right) at 80 m. The template based method is in good agreement with the model hindcast. The spatial patterns are quite similar, both showing lee effects to the SE of the island. The largest differences, south of Block Island are an over prediction of the wind speed of about 0.4 m/sec or about 3.5 % of the 10.2 m/sec winds. For power the template method predicts more pronounced lee effects from NW winds compared to the hindcast. The largest difference is on the order 100 kW/m^2 south of Block Island or 12% higher than the mean value.

Figure 26 shows the observed and hindcast wind roses at AWS Met 57 m. The model hindcast under predicts the winds from the NW and over predicts those from the W. This is particularly the case at higher wind speeds. This explains why the template derived results show a more pronounced lee effect to the SE than the hindcast.

To investigate this issue further, the template method was applied again but using the hindcast wind at the AWS Met site, rather than the observed values at this location. This estimate hence removes the difference in wind roses between the hindcast and observations and focuses on the just difference between the hindcast and template methods. Figure 27 shows the template (upper panel), hindcast (center panel), and difference between the two (lower panel) for the mean wind speeds (left) and power (right) at 80 m. Comparing to Figure 26, the template method predictive performance is measurably improved. The differences in mean wind speed have been reduced from 0.2 to 0.4 m/sec to 0.1 to 0.2 m/sec. Similar reductions in the differences are also observed for wind power; from 100 kW/m^2 to 60 kW/m^2.

7. Conclusions

The major conclusions from this study are:

NW and NE dominate the observed winds at MDS and AWS Met for this fall - winter study period. This pattern is consistent with wind hindcasts for the winter from the nearby WIS 101 site. The wind speeds increase with height and have low shear coefficients, consistent with unstable atmospheric conditions. The Weibull distribution shape parameter is approximately 2.12 and the amplitude parameter increases with observation height.

Model predicted wind speeds are in good agreement with observations for temporal trends. The model under predicts the observed wind speed at 57 m elevation at the AWS Met station by an average difference of 5.1% (Obs. - 9.73 m/sec vs RAMS -9.23 m/sec.). The model similarly under predicts the observed power at this location by 16.1 % (Obs. - 1000 kW/m^2 vs RAMS - 838 kW/m^2). RAMS predicted values at MDS (10 m elevation) are in good agreement with

observations (Obs – 8.54 m/sec versus RAMS – 8.23 m/sec), under predicting the wind speed by 5.7 %.

Model predicted wind speeds and power density distributions show the same basic pattern: shore parallel contours with speed or power density increasing with distance offshore. Regions to the S and SE of Block Island represent oceanic wind conditions, while those to the N and NW are strongly influenced by the adjacent land masses. The simulations show substantial lee effects that are predicted to extend at least 8 km from the island at 80 m. The location of the impacted area is dependent on the wind direction, lee effects SE of the island result from NW winds and SW for NE winds. The lee effects are most pronounced from the southern end of the island, which has the highest elevation and the highest roughness land cover. Model predicted shear coefficients are higher (0.18) than the observed values (0.08) at AWS Met. Shear coefficients are very large over the island reaching values as high as 0.45 on the southern end.

A sensitivity study was performed to assess the impact on winds in the lee of Block Island for NW winds assuming the island both topography and land cover, or each independently were used as input to the model. The simulations showed that either topography or land cover alone explained much of the observed lee effects.

Mean powers densities were predicted for a small wind farm located at the state water boundary line. The site locations and their power densities are: SE- 1097 kW/m^2, S - 1139 kW/m^2, and SW -1076 kW/m^2. The S site has the highest power production potential; 3.6 to 5.4 % higher than the other two sites. The SW has been eliminated from consideration based on high construction effort due to end moraine sediments. Of the two remaining sites, the S site has a marginally higher power production potential than the SE site. It should be noted that this analysis has not considered winds from other times of the year. During the remainder of the year, winds are observed to be predominantly from the SW. With SW winds all three locations are anticipated to experience about the same winds and hence power production potential. The simulations are for one fall and winter season and cover a time period when winds from the NE were significantly more frequent than climatological means, while the winds from the NW, the direction of particular interest, were typical.

Simulations for the hindcast period were compared to application of an independent template based method for the study period. The results showed the template based predictions were in generally good agreement with the hindcast mean winds, and correctly predicted the lee effects from both NW and NE winds. The template based method showed a more pronounced lee area to the SE. The predictive quality for wind power was comparable. A comparison of the observed and hindcast wind rose show the model under predicts the winds from the NW and over predicts those from the W, hence explaining in part the difference between the two estimates.

References

Alessandrini, S, G. Decimi, L. Palmieri, and E. Ferrero, 2009. A wind power forecast system in complex topographic conditions, Proceedings of 2009 European Wind Energy Conference (EWEC), Marseille, France.

ATM, 2007a. RI WINDS Phase I, Wind Energy Siting Study, prepared for RI Office of Energy Resources, Providence, RI, April 2007.

ATM, 2007b. RI WINDS Summary Report, prepared for RI Office of Energy Resources, Providence, RI, September 2007.

Brower, M., 2007. Wind resource maps of Southern New England, prepared by True Wind Solutions, LLC, 10 p.

Castellani, F, C. Busillo, F. Calastrini, G. Gualtieri, G. Molina, and L. Terzi, 2007. An hybrid approach for downscaling rams data for wind resource assessment in complex terrains, Proceedings of 2007 European Wind Energy Conference (EWEC).

Guenard, V, 2008, Wind resource assessment with a meso-scale non-hydrostatic model, Proceedings of 2008 European Wind Energy Conference (EWEC).

Grilli, A. M. L. Spaulding, C. Damon, and R. Sharma, 2010. High resolution application of the Technology Development Index (TDI) in state waters south of Block Island, Ocean SAMP project Report, Narragansett, RI.

Freedman, J. M. and M. Markus, 2010. Report on Block Island wind resource assessment methodologies and modeling sensitivity studies, AWS True Winds LLC, Albany, NY.

Pielke, R.A., W.R. Cotton, R.L. Walko, C.J. Tremback, W.A. Lyons, L.D. Grasso, M.E. Nicholls, M.D. Moran, D.A. Wesley, T.J. Lee, and J.H. Copeland, 1992: A comprehensive meteorological modeling system -- RAMS. Meteor. Atmos. Phys., 49, 69-91.

RAMS, 2010, Regional Atmospheric Modeling System Technical Manual, Weather Flow,

Spaulding, M. L., A. Grilli, C. Damon, and G. Fugate, 2010a, Application of Technology Development Index and Principal Component Analysis and Cluster Methods to Ocean Renewable Energy Facility Siting, Journal of Marine Technology, Special Edition on Offshore Wind, January February 2010.

Spaulding, M.L., M. Bell, J. Titlow, R. Sharma , A. Grilli, A. Crosby, L. Decker and D. Mendelsohn, 2010b. Wind Resource Assessment in the Vicinity of a Small, Low Relief Coastal Island, University of Rhode Island, Narragansett, RI 02882.

Sukegawa, H., T. Ishihara, A. Yamaguchi, and Y. Fukumoto. 2006. An Assessment of Offshore Wind Energy Potential Using Mesoscale Model, Proceedings of 2006 European Wind Energy Conference (EWEC).

Titlow, J. and D. Morris, 2010. Block Island modeling analysis, WeatherFlow Inc. Model simulations by MetLogics, Boulder, CO.

Tremback, C. J. and R. L. Walko, 2010. Regional Atmospheric Modeling System, Users Guide-Introduction, Version 6.0, ATMET, Boulder, CO

Walko, R.L., L.E. Band, J. Baron, T.G.F. Kittel, R. Lammers, T.J. Lee, D. Ojima, R.A. Pielke Sr., C. Taylor, C. Tague, C.J. Tremback, and P.L. Vidale. 2000. Coupled atmosphere-biophysics-hydrology models for environmental modeling. Journal of Applied Meteorology 39(6): 931-944.

Wensong, Weng, Peter A. Taylor, James R. Salmon, 2010. A 2-D numerical model of boundary-layer flow over single and multiple surface condition changes, Journal of Wind Engineering and Industrial Aerodynamics, Volume 98, Issue 3, March 2010, Pages 121-132, ISSN 0167-6105, DOI: 10.1016/j.jweia.2009.10.006.

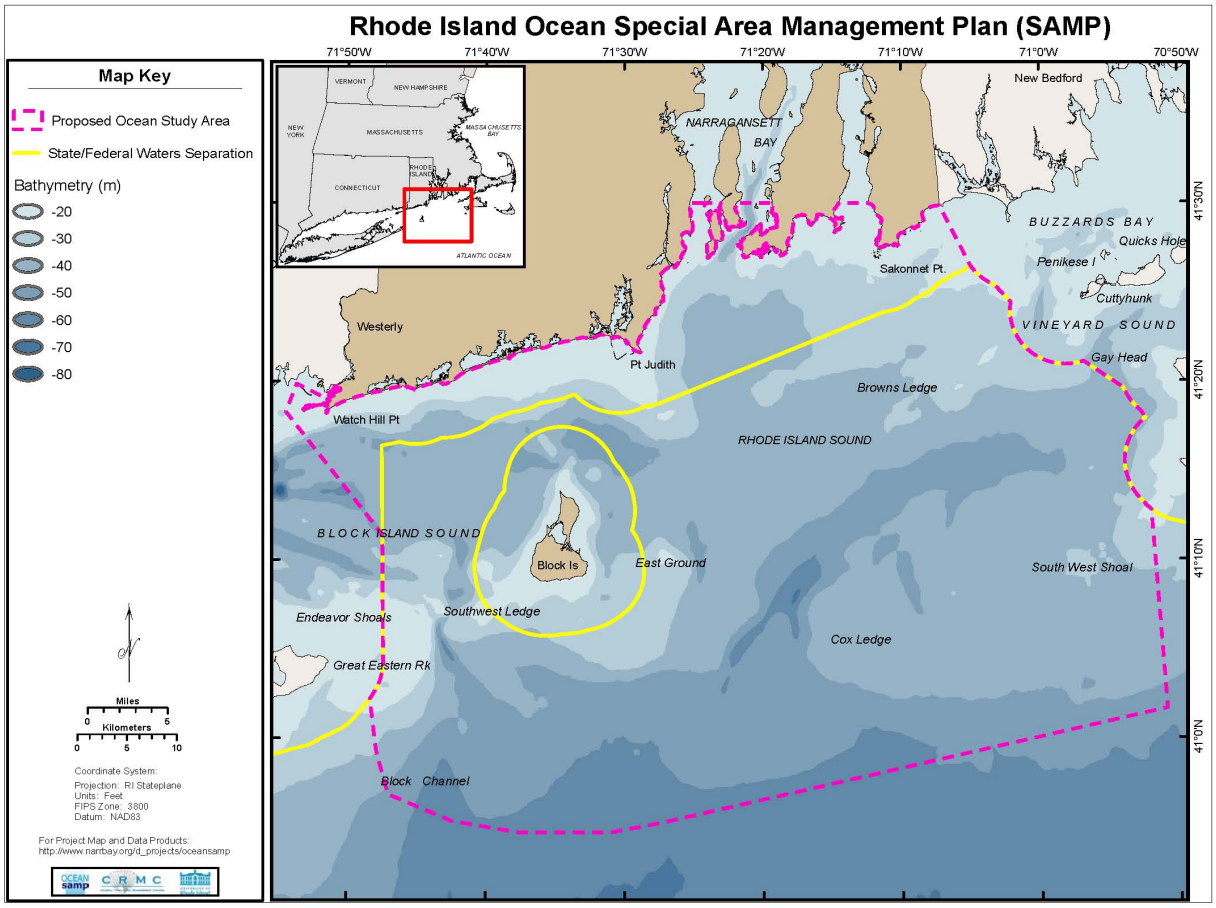

Figure 1 Ocean SAMP study area with bathymetry as background. Yellow lines are state water boundaries and dotted lines are study area boundaries.

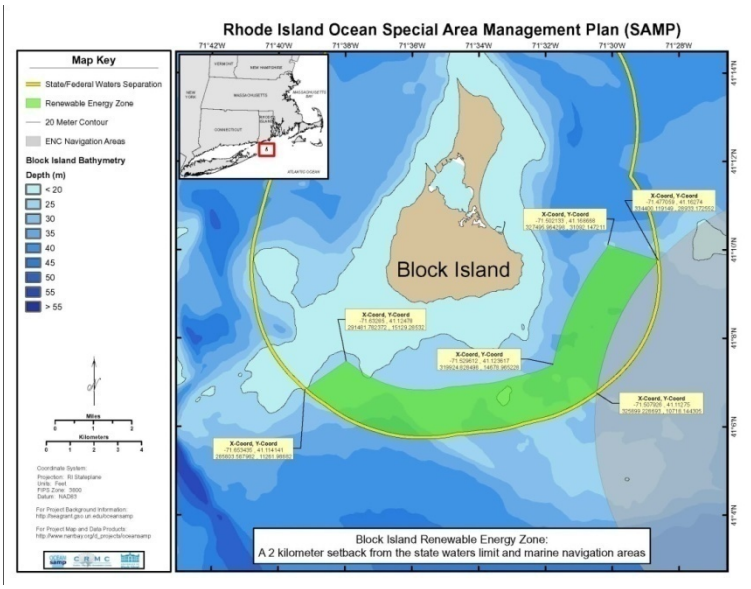

Figure 2 Proposed renewable energy zone south of Block Island. Latitude and longitude (state plane) coordinates are provided at key points.

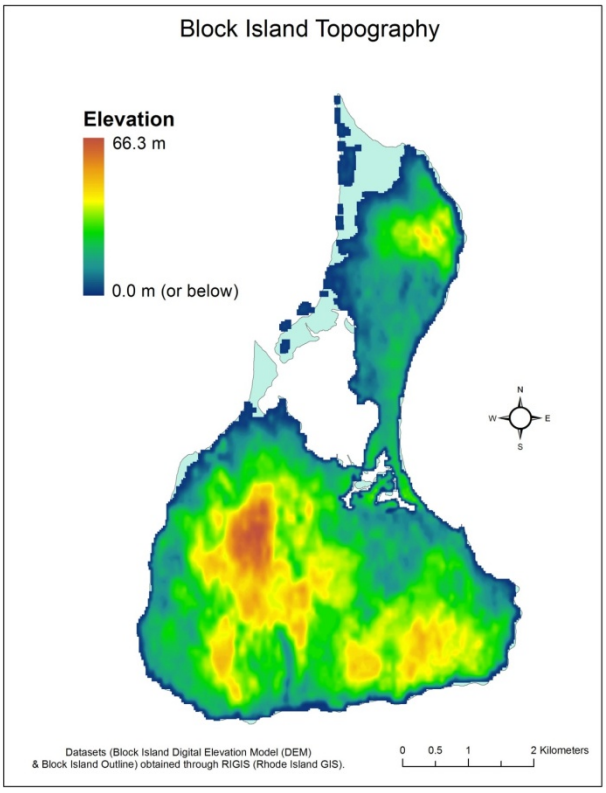

Figure 3 Block Island topography based on RI GIS digital elevation maps.

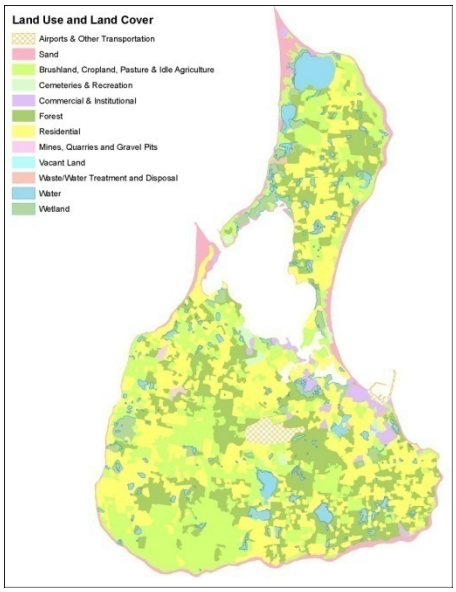

Figure 4 Block Island land cover (RI Geographic Information System).

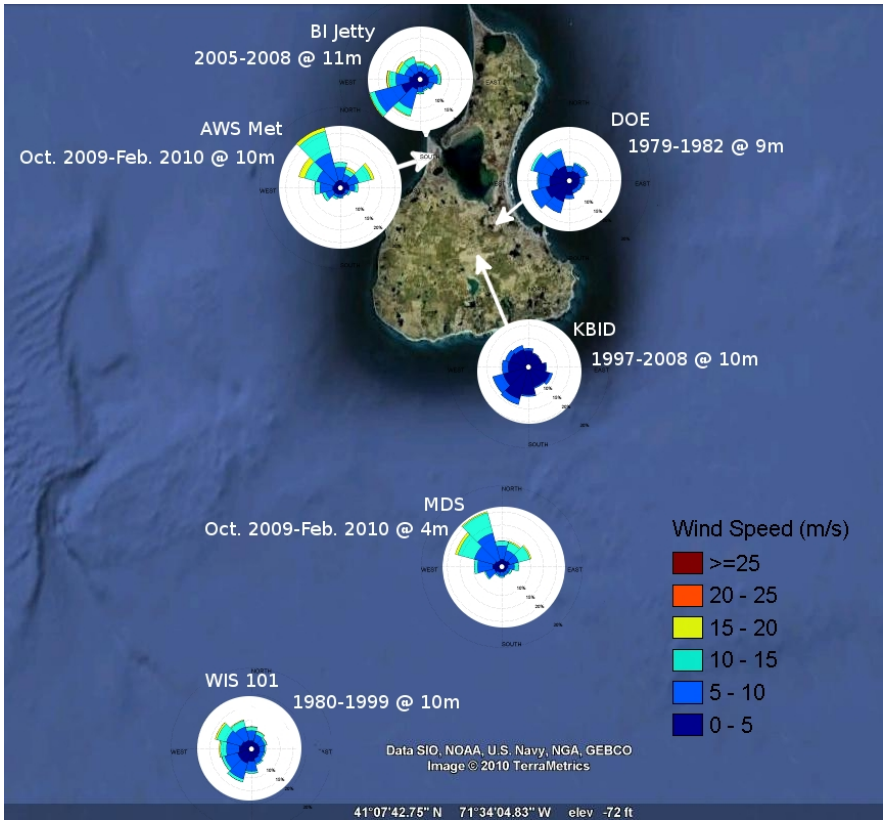

Figure 5 Wind speed frequency rose at AWS Met and MDS stations. Data is also shown for WIS101, Block Island Airport (KBID), DOE and WeatherFlow's Block Island Jetty.

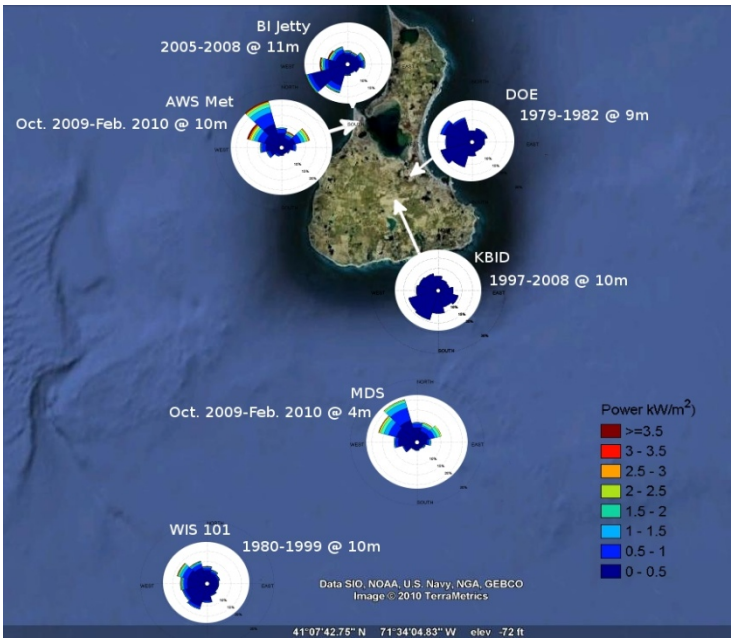

Figure 6 Wind power roses at AWS Met and MDS stations. Data is also shown for WIS101, Block Island Airport (KBID), DOE and WeatherFlow's Block Island Jetty.

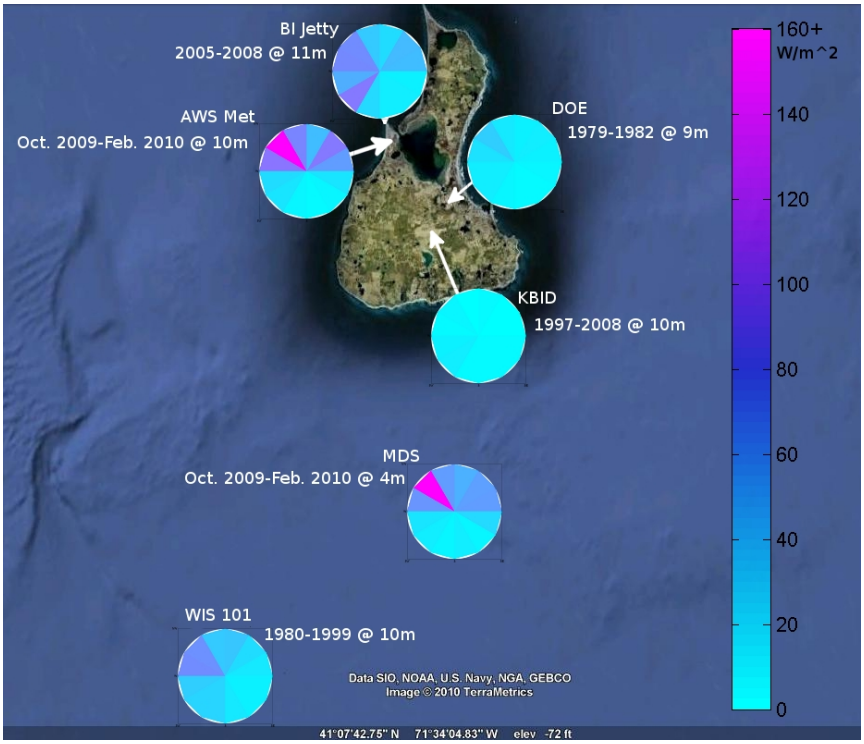

Figure 7 Average wind power by direction. Data is also shown for WIS101, Block Island Airport (KBID), DOE and WeatherFlow's Block Island Jetty.

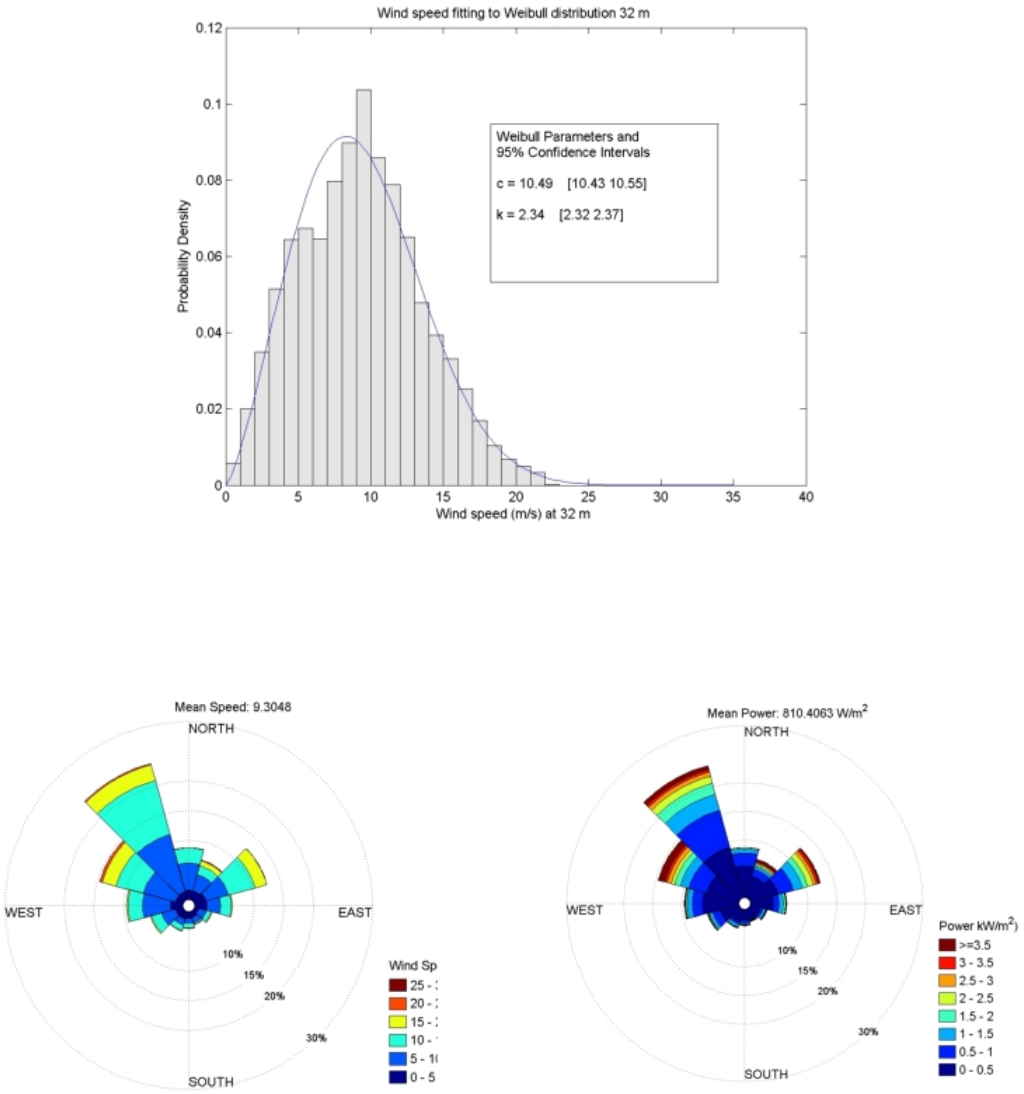

Figure 8 Weibull distribution, wind frequency and power roses for AWS Met, 32 m elevation.

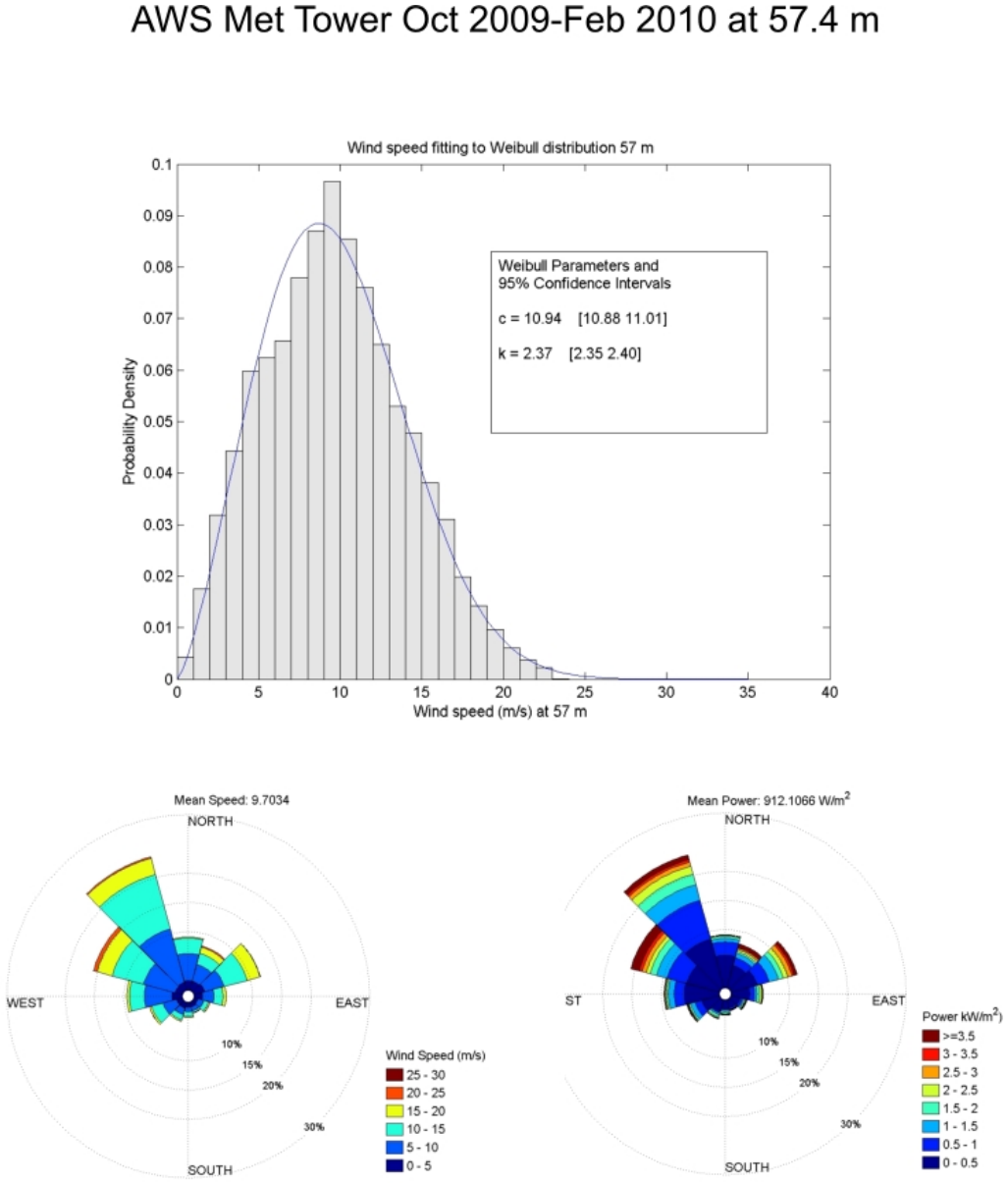

Figure 9 Weibull distribution, wind frequency and power roses for AWS Met, 57 m elevation.

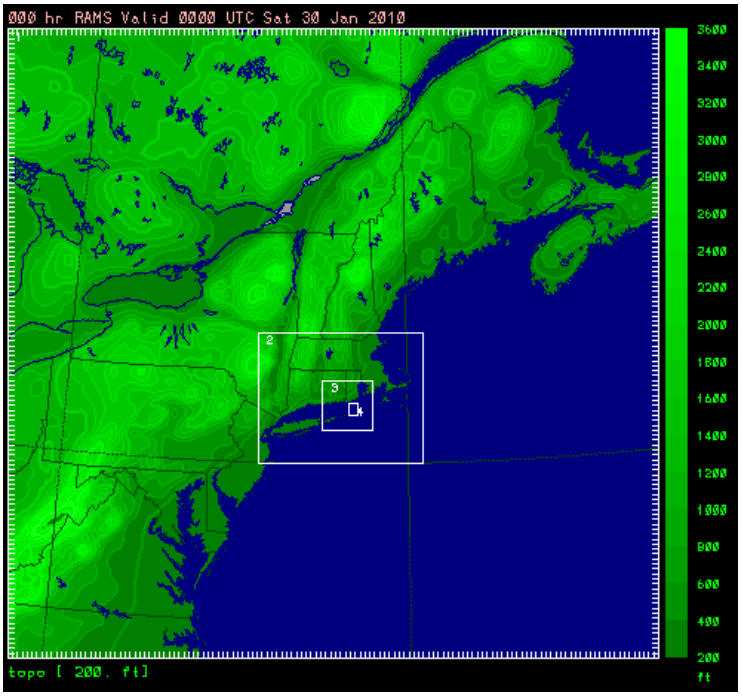

Figure 10 RAMS nested grid system showing 6 km (Grid 2), 2 km (Grid 3) and 0.5 km (Grid 4) grid boundaries. The outer NCEP NAM grid is 12 km.

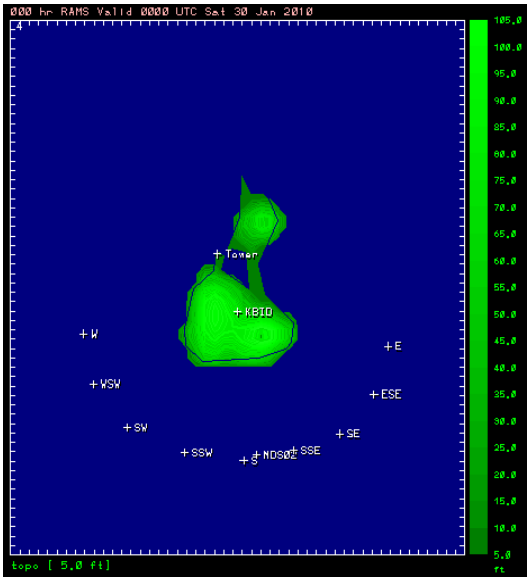

Figure 11 Grid 4 showing topographic relief of Block Island. The locations at which model time series were generated are shown, including E, ESE, SE, SSE, S, SSW, SW, WSW, and W along state water boundary line, and at observation locations KBID, BI Jetty, AWS Met, and MSD.

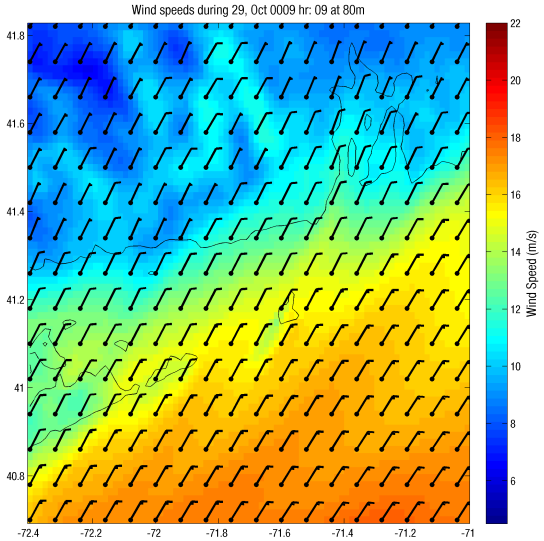

Figure 12a Model predicted wind speed contours (Grid 3) on October 29, 2009 at 80 m elevation on Grid 3. Wind barbs are provided to show wind direction.

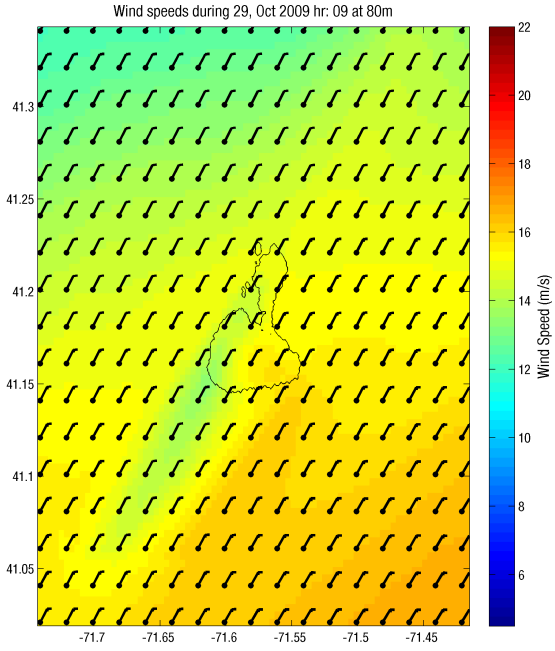

Figure 12b Model predicted wind speed contours (Grid 4) on October 29, 2009 at 80 m elevation on Grid 4. Wind barbs are provided to show wind direction.

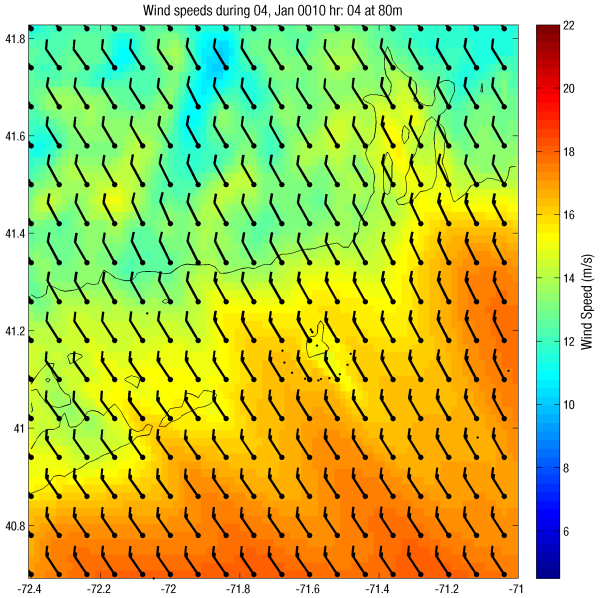

Figure 13a Model predicted wind speed contours (Grid 3) on January 4, 2010 at 80 m elevation. Wind barbs are provided to show wind direction.

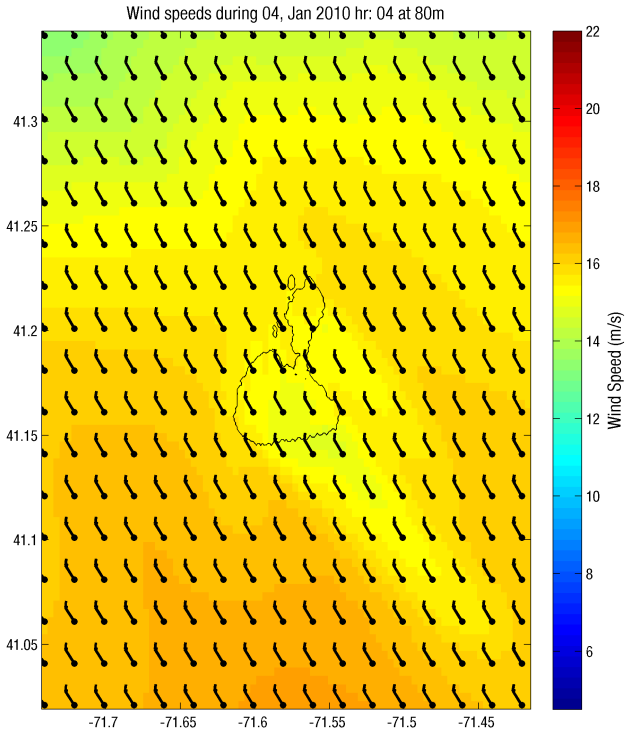

Figure 13b Model predicted wind speed contours (Grid 4) on January 4, 2010 at 80 m elevation. Wind barbs are provided to show wind direction.

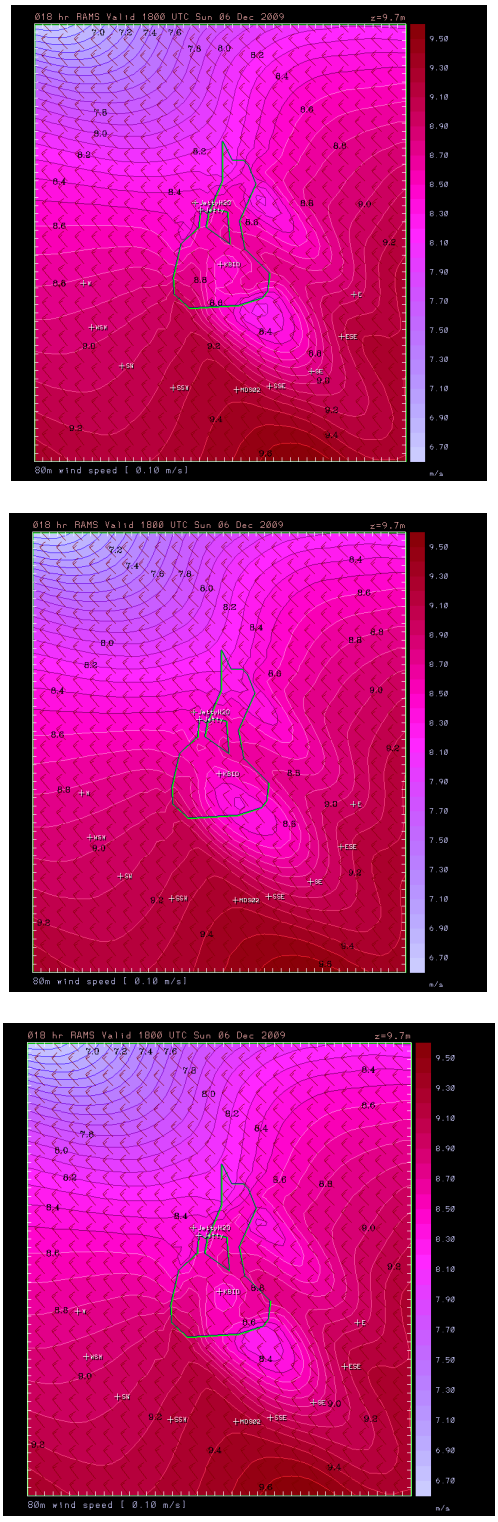

Figure 14 Model predicted wind field on December 6, 2009, 80 m elevation with topography and roughness (upper panel), with roughness only (center panel) and with topography only (lower panel).

Figure 15 Model predicted and observed wind speed vs time (upper panel) and difference between the two (lower panel)(blue - observed, red - model) for the simulation period at AWS Met at 57 m elevation.

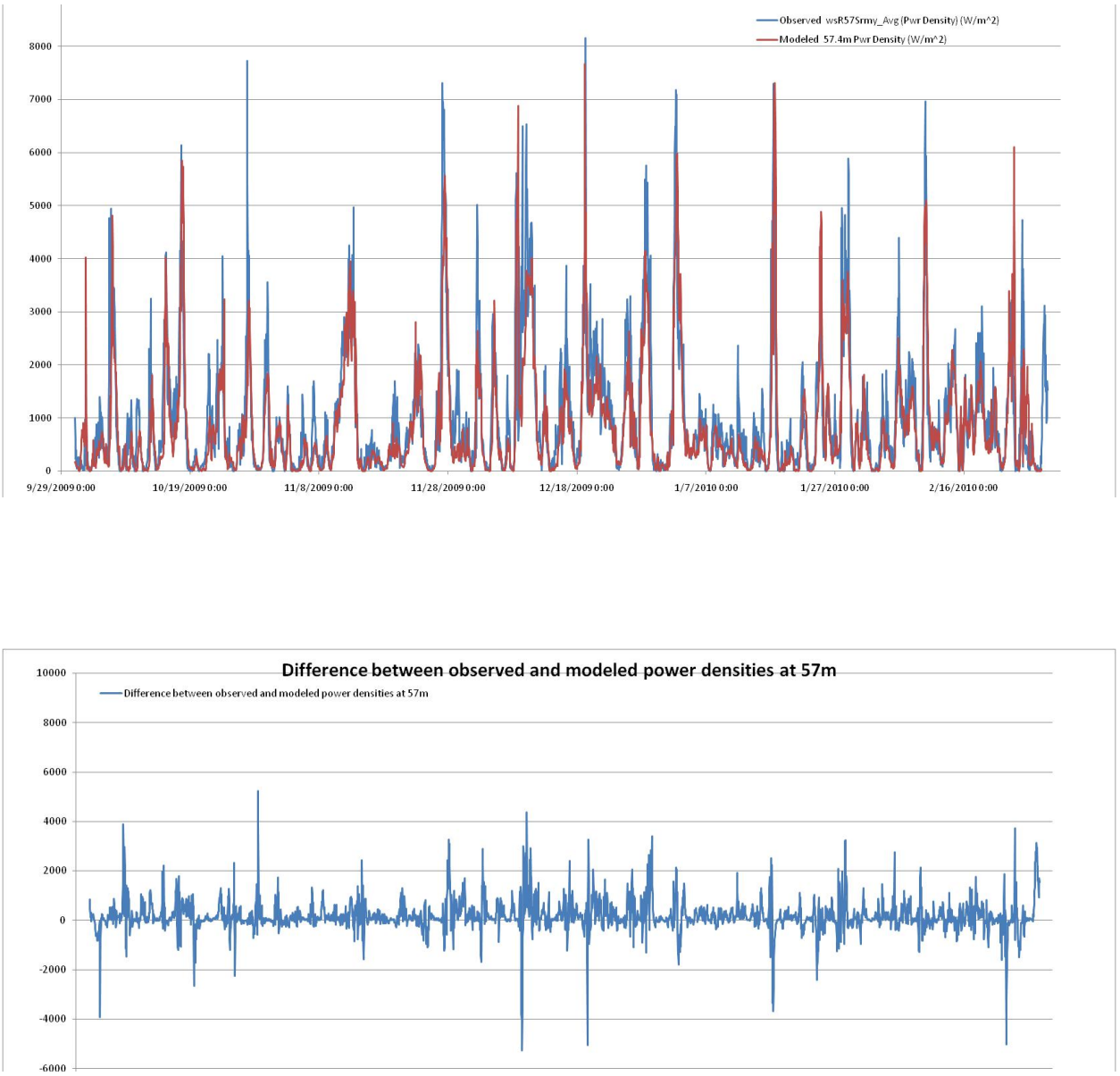

Figure 16 Model predicted and observed power density vs time (upper panel) (blue - observed, red-model) and difference between the two (lower panel) at the AWS Met 57 m elevation.

Figure 17 Model predicted and observed shear vs time (upper panel)(blue –observed, red- model) and difference between the two (lower panel) at the AWS Met 57 m elevation.

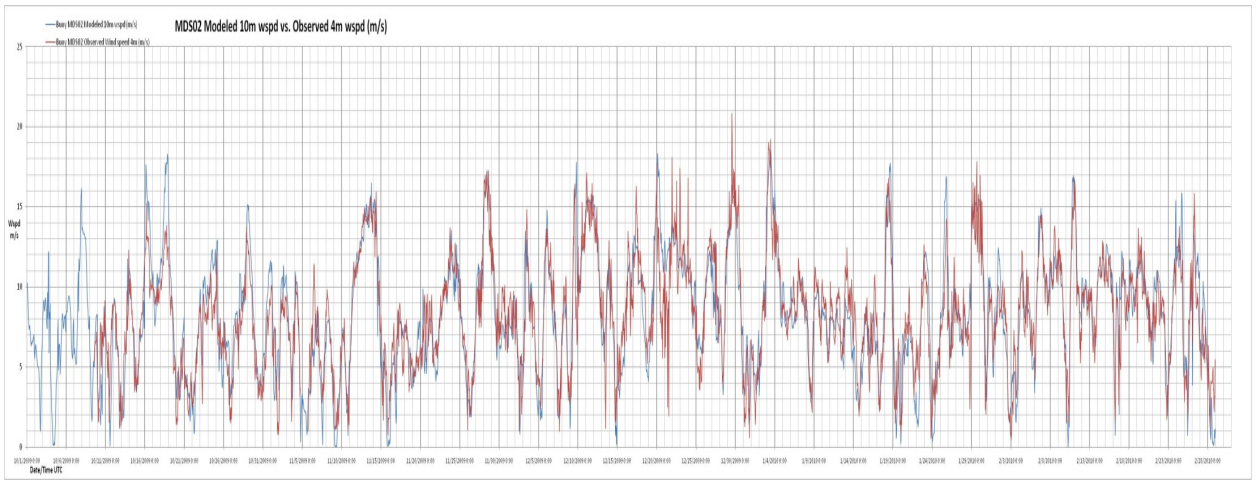

Figure 18 Model (red) predicted and observed (blue) winds at MDS at 10 m elevation.

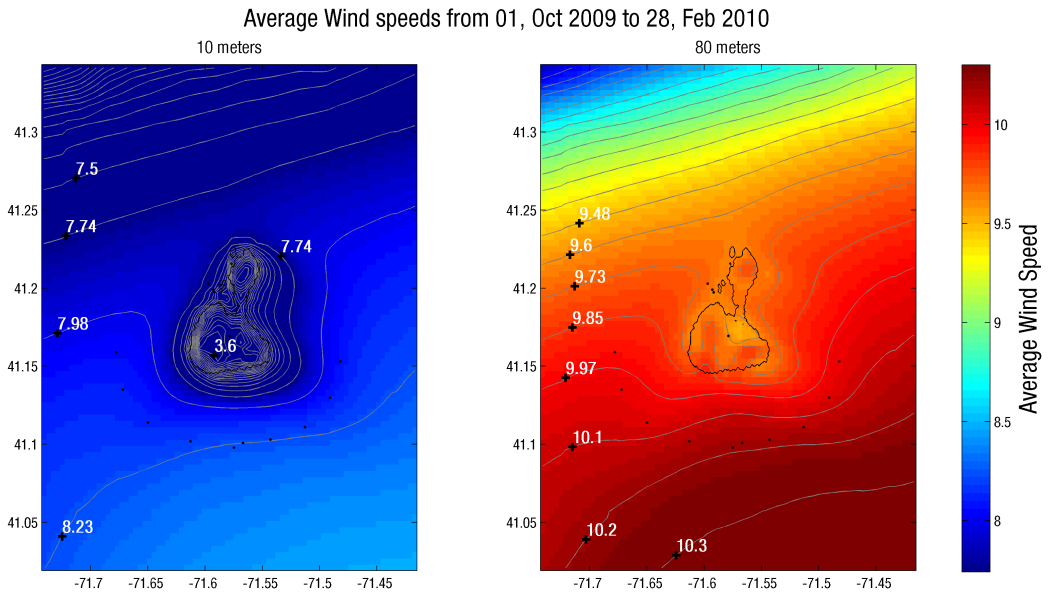

Figure 19 Average model predicted wind speed contours at 10 m (left) and 80 m (right) elevations over the simulation period.

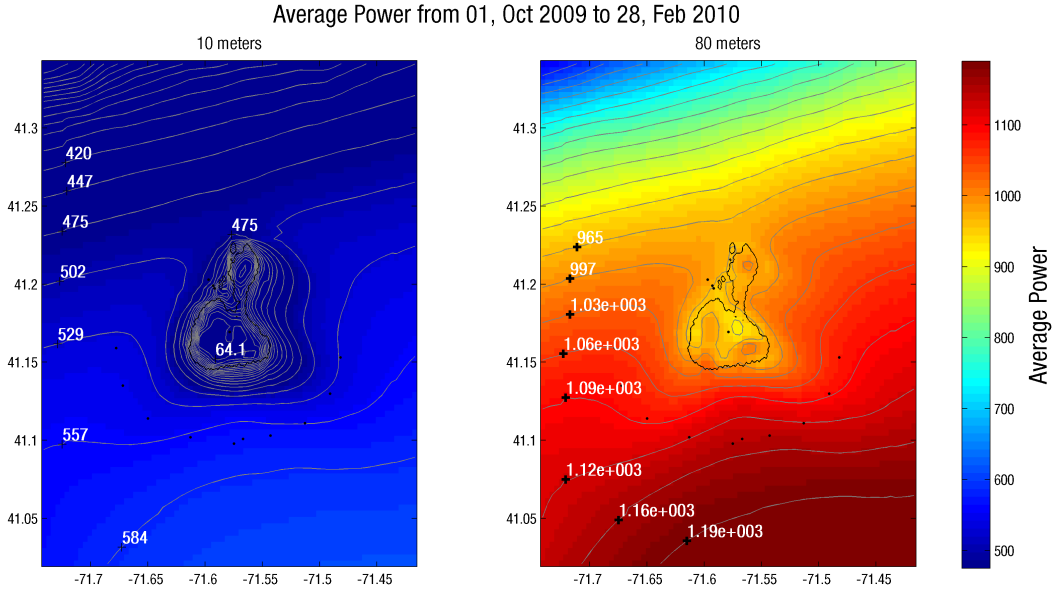

Figure 20 Average model predicted wind power (kW/m^2)contours at 10 m (left) and 80 m (right) elevations over the simulation period.

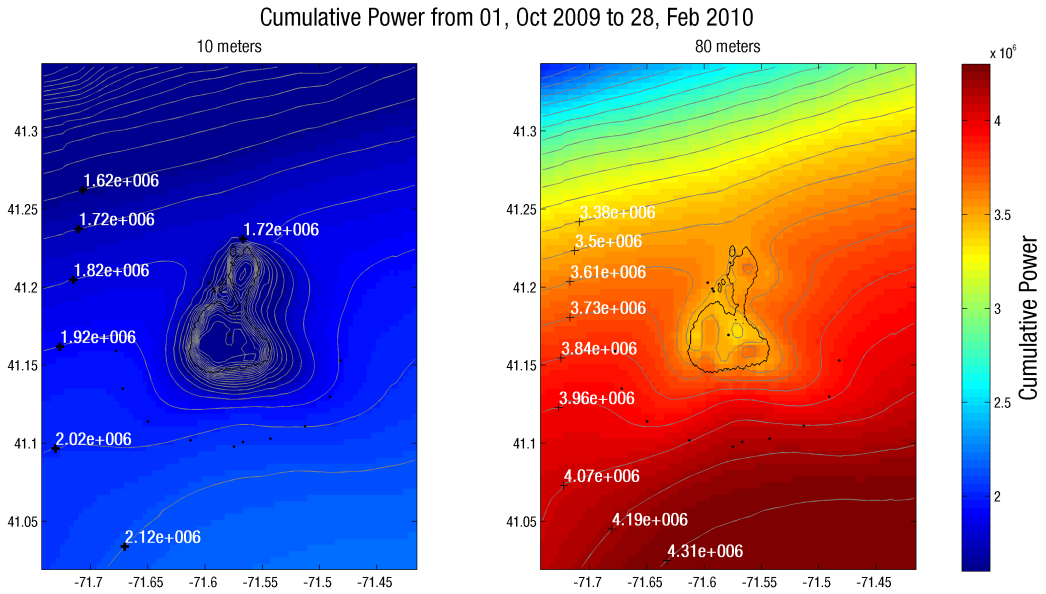

Figure 21 Average model predicted cumulative wind power (kW hrs/m^2) contours at 10 m (left) and 80 m (right) elevations.

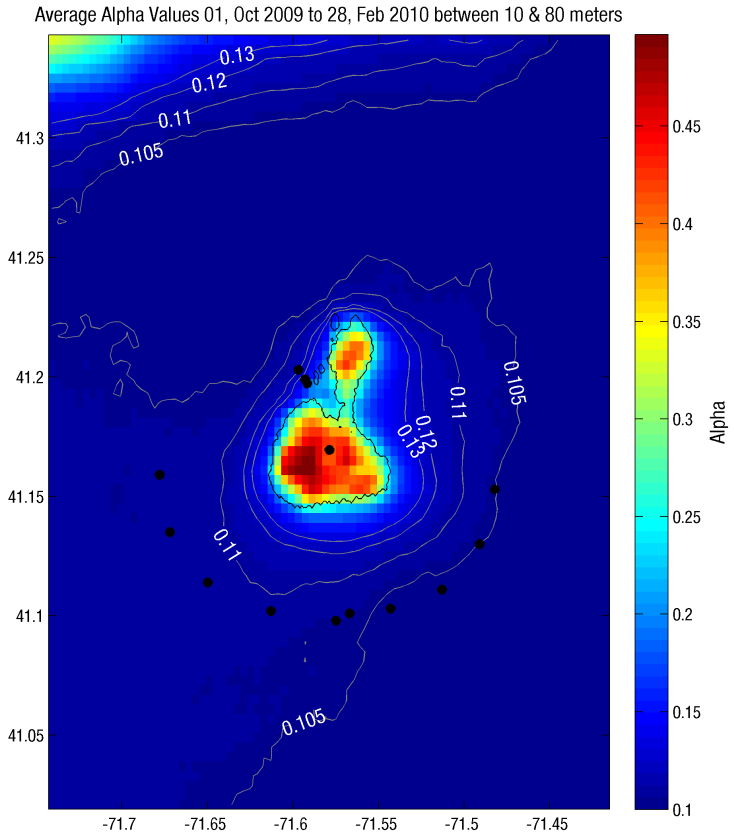

Figure 22 Model predicted average shear coefficient over the simulation period.

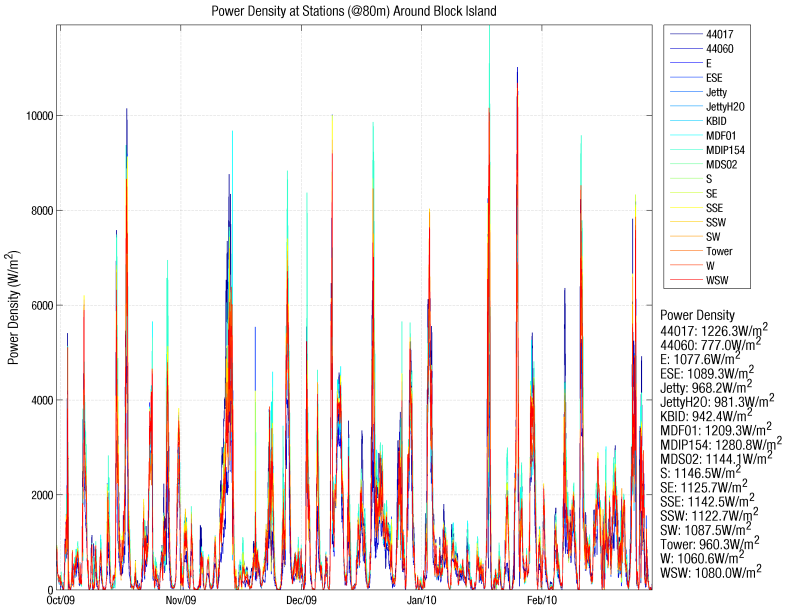

Figure 23 Model predicted time series of wind power density at selected sites (see Figure 11)

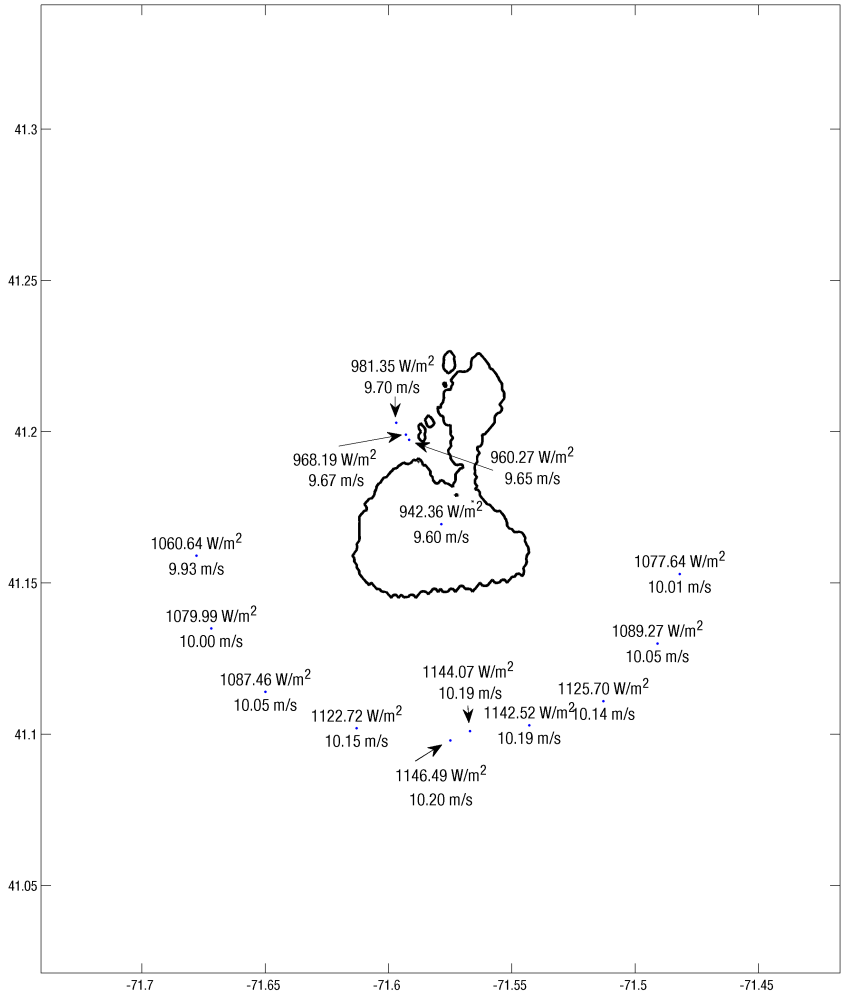

Figure 24 Model predicted mean wind power density at selected sites (see Figure 11)

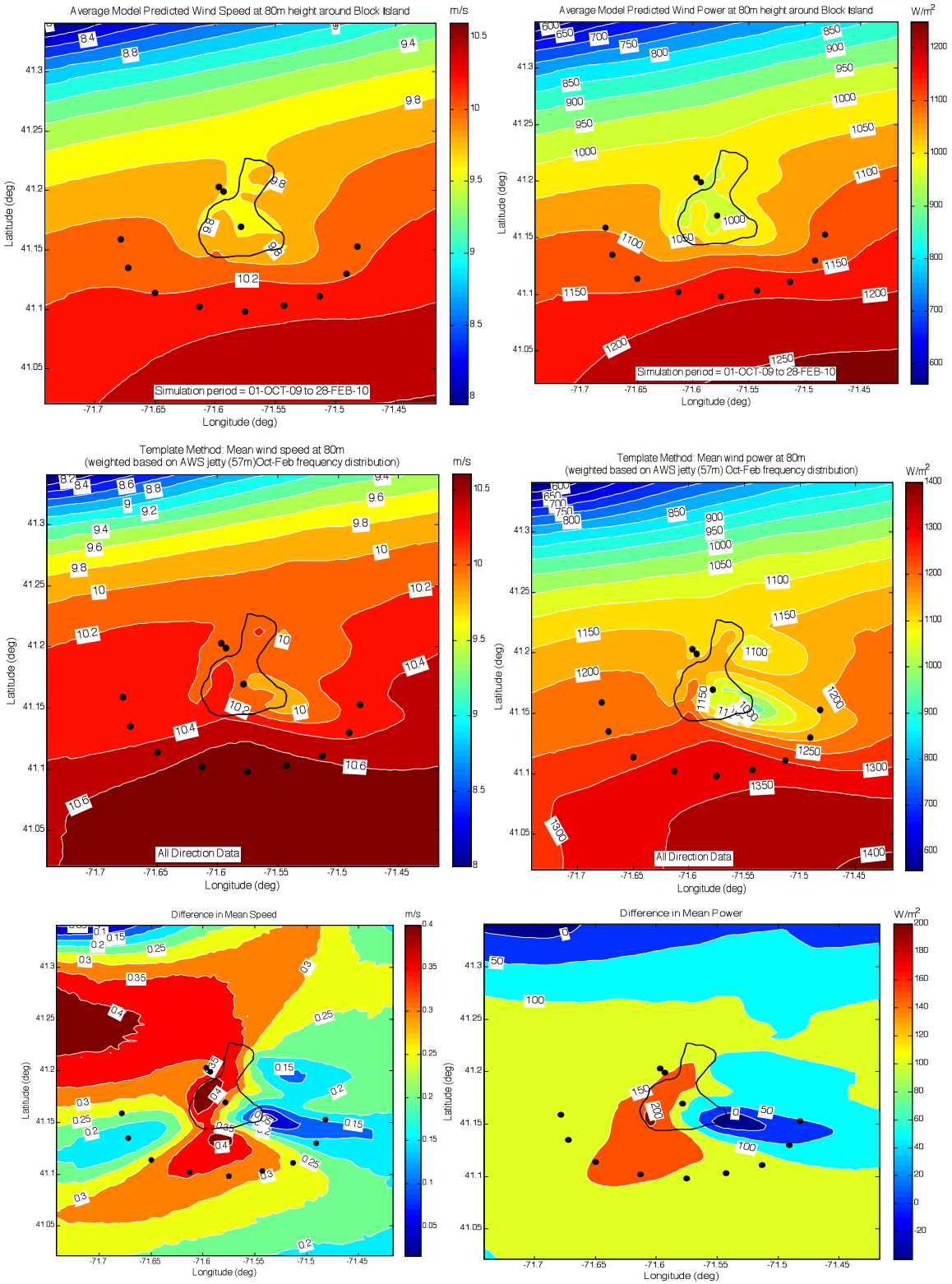

Figure 25 Mean wind speed (left) and power (right) at 80 m based on the template method (using AWS Met wind rose at 57m) (Spaulding et al, 2010b) (upper panel), present hindcast (center panel), and difference between the two methods (lower panel).

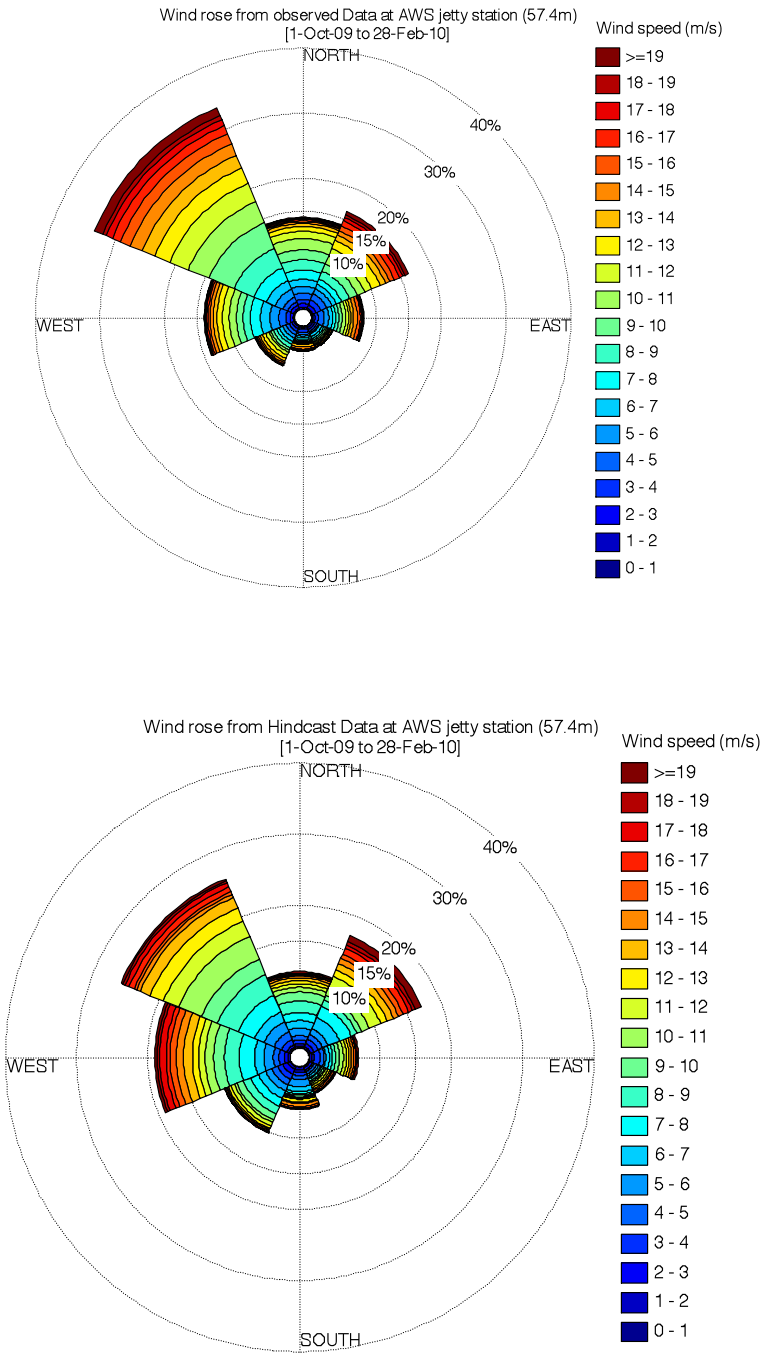

Figure 26 Observed (upper panel) and hindcast (lower panel) wind speed rose at AWS Met 57 m elevation.

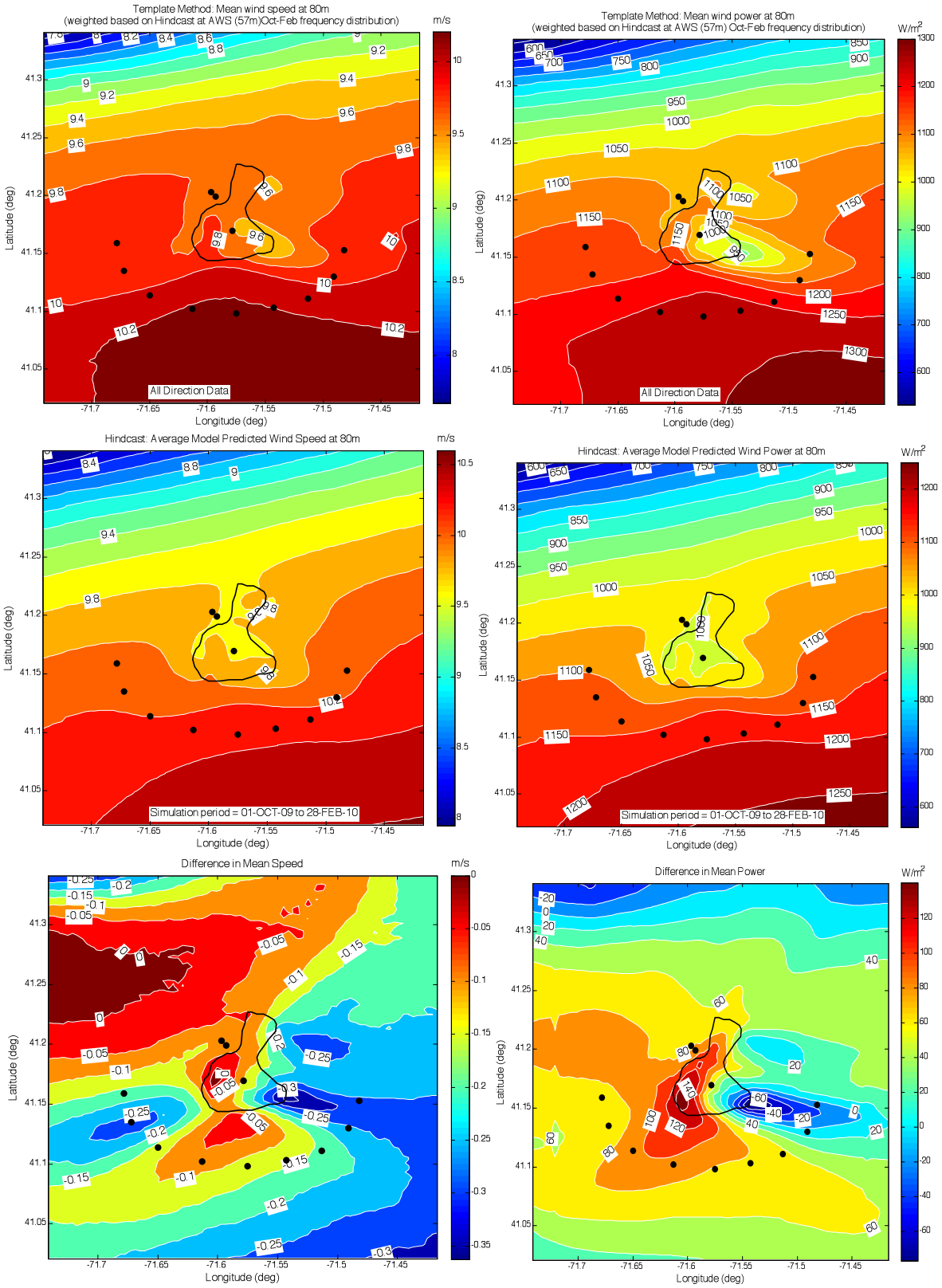

Figure 27 Mean wind speed (left) and power (right) at 80 m based on the template method (using hindcast wind rose at AWS Met location) (Spaulding et al, 2010b) (upper panel), present hindcast (center panel), and difference between the two methods (lower panel).

Appendix A

Titlow, J, 2010. Comparison of RAMS Model Predictions with Observations for the October 2009 to February 2010 Hindcast Period, WeatherFlow Inc., Poquoson, VA.

Appendix A is a twenty-seven slide Power Point presentation avialable on request from the frist author.

Appendix B

Comparison Weather Flow Simulations and Observations at AWS Met tower

Data

Observations

Period of record: 10/01/2009 to 28/02/2010

Sampling interval : 10 minutes

Data: wind speed at 32.1 m and 57.4 m

Observations at each level are used to infer the "observed" shear coefficient which is used to derive the "observed" wind speed and power at 80 m.

Modeled data

Period of simulation: 10/01/2009 to 28/02/2010

Time step: 1 hour

Data: wind speed at 32.1 m , 57.4 m, 80 m, shear coefficient, power at 80 m

Data analysis

1. Time series preparation

Observed data are smoothed and rei-interpolated on 1 hour time step to be synchronized with Weather Flow modeled data at each measurement level (Figure 1 and Figure 2). Visual comparison show a slight time lag between observation and simulations (about 5h). This lag is due to the fact the model predictions are provided in UTC and the observations in EST, a 5 hr time difference.

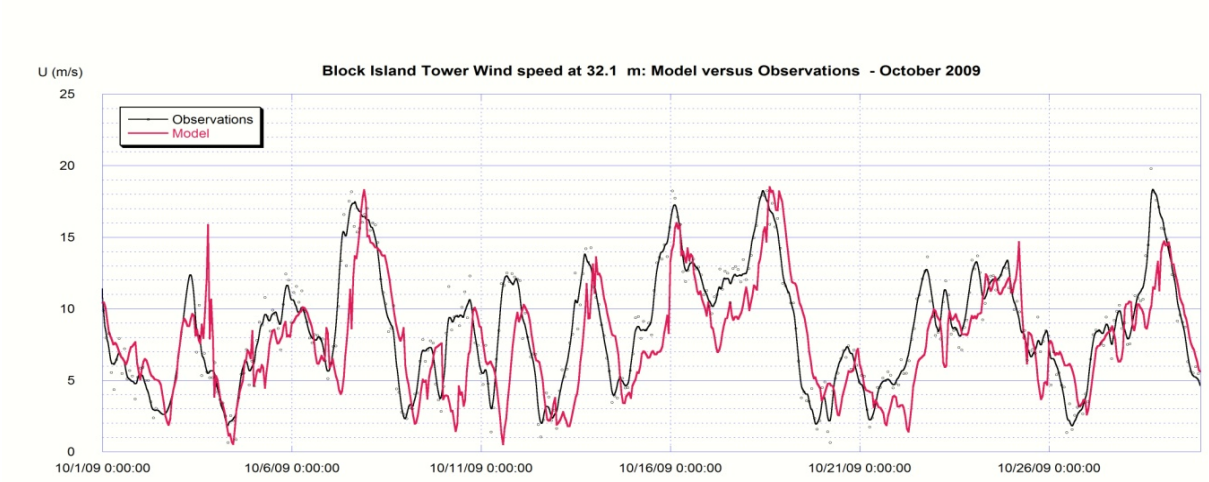

Figure 1: Time series of observed and modeled wind speed at 32.1 m at Block Island AWS Met Tower- Example for October 2009.

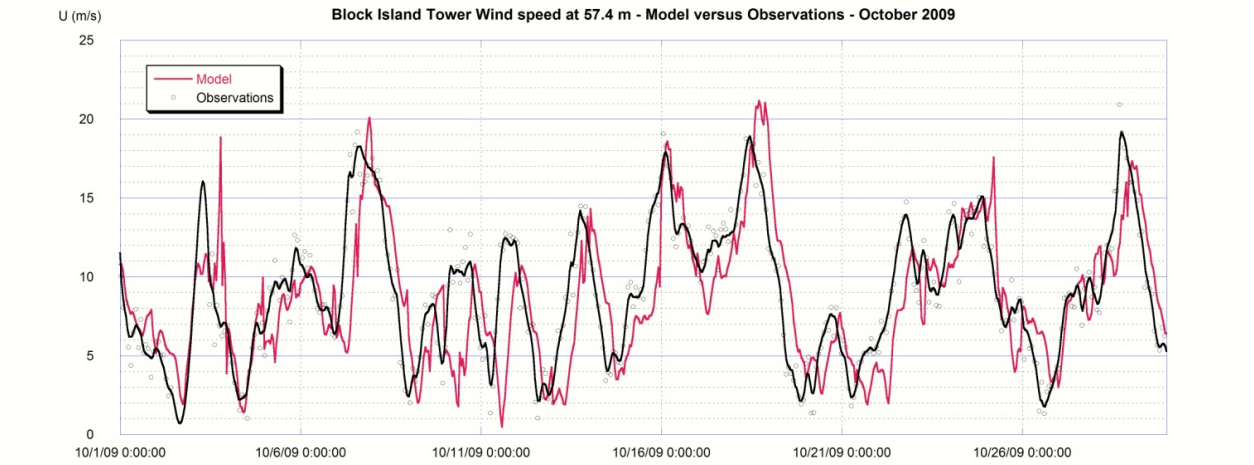

Figure 2: Time series of observed and modeled wind speeds at 57.4 m at Block Island Met Tower - Example for October 2009

2. Cross-correlation analysis

The Cross correlation coefficient function is calculated for each pair, observations-simulations : wind speed at at 32.1 m, 57.4 m , and 80 m, shear coefficient , wind power at 80 m. The function measures the degree of linear dependence between the 2 time series for any relative displacement τ , between them . Results are plotted for each pair for a range of τ between 0 and +- 20 (hours). The peak shows the optimal value of the correlation for the corresponding time lag. A consistent time lag of 5 hours is found between the 2 time series which is consistent with Figure 1 and Figure 2. The correlation coefficient is above 90% for wind speeds observations versus simulations, and 86% for simulated versus "observed" wind power at 80 m. The shear coefficient however is in poor agreement with a correlation coefficient of 0. 47.

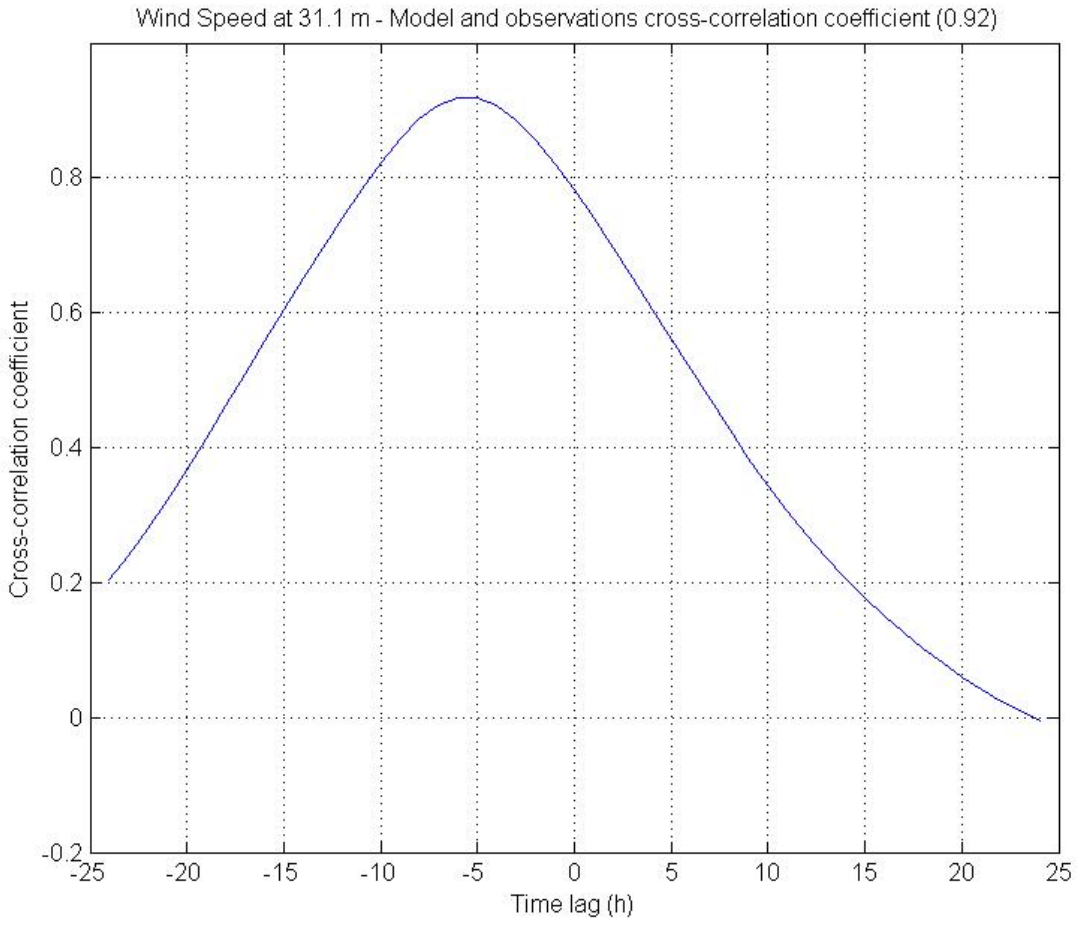

Figure 3: Cross-correlation coefficient for modeled and observed wind speeds at 32.1 m at Block Island AWS Met Tower.

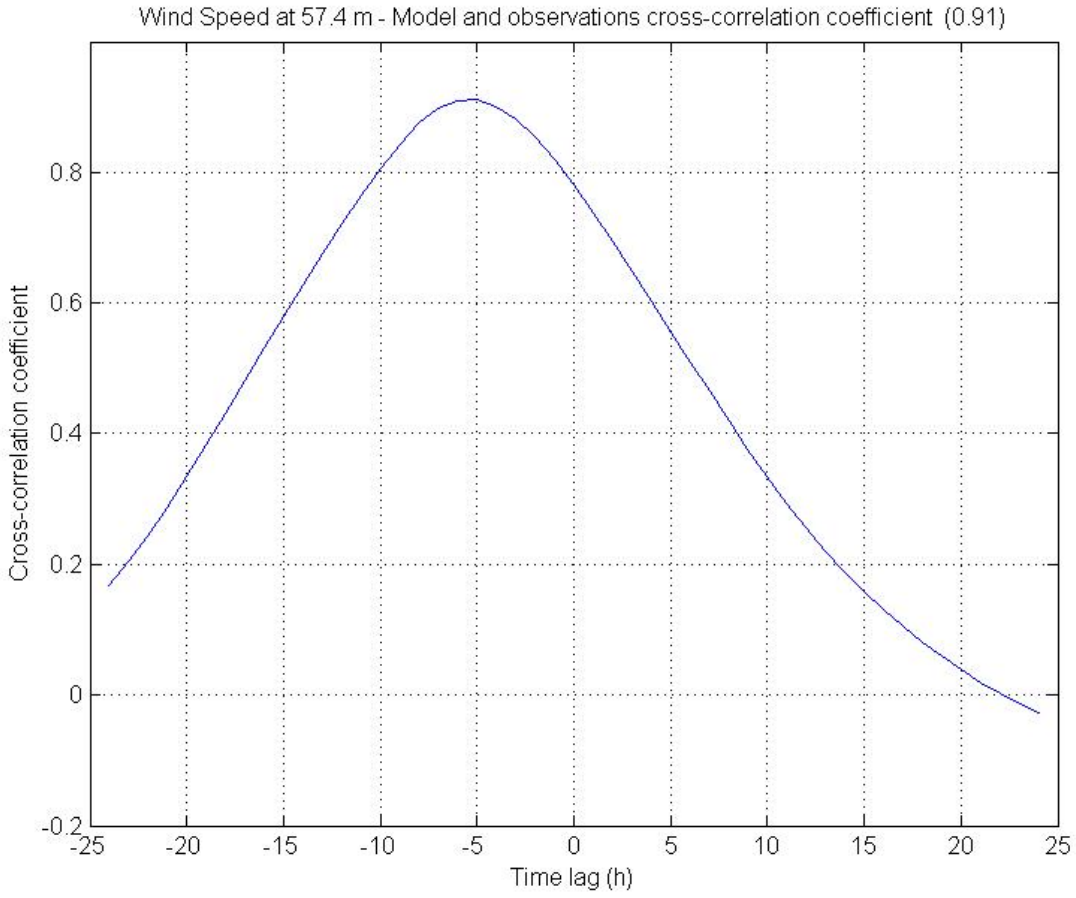

Figure 4: Cross-correlation coefficient for modeled and observed wind speeds at 57.4 m at Block Island AWS Met Tower.

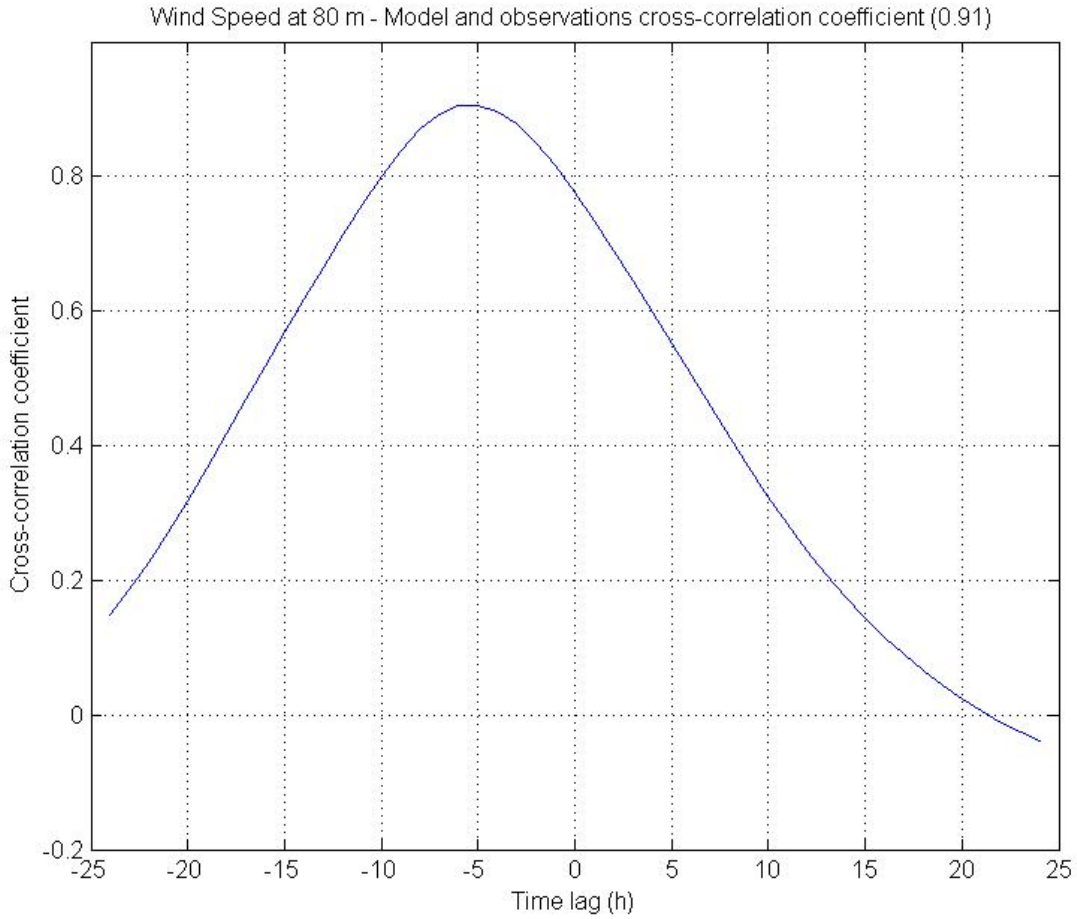

Figure 5:Cross-correlation coefficient for modeled and observed wind speeds at 80 m at Block Island AWS met Tower.

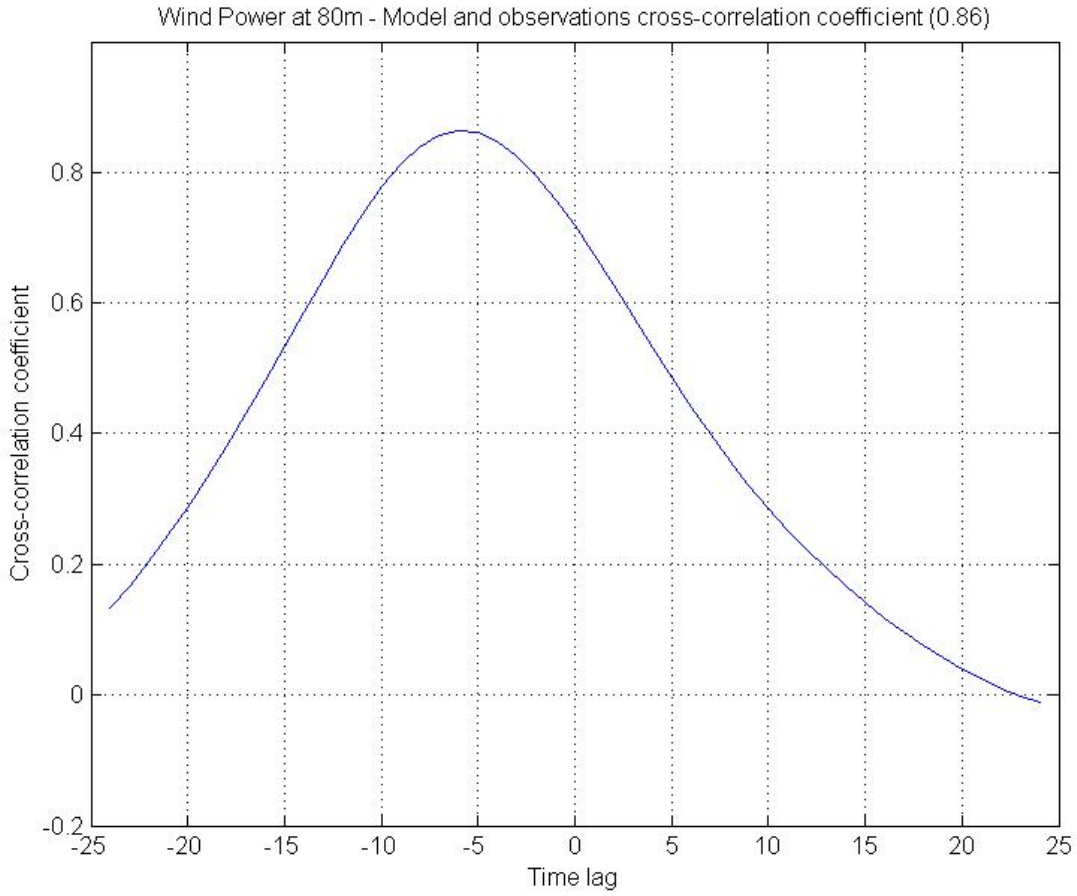

Figure 6:Cross-correlation coefficient for modeled and observed wind powers at 80 m at Block Island AWS met Tower.

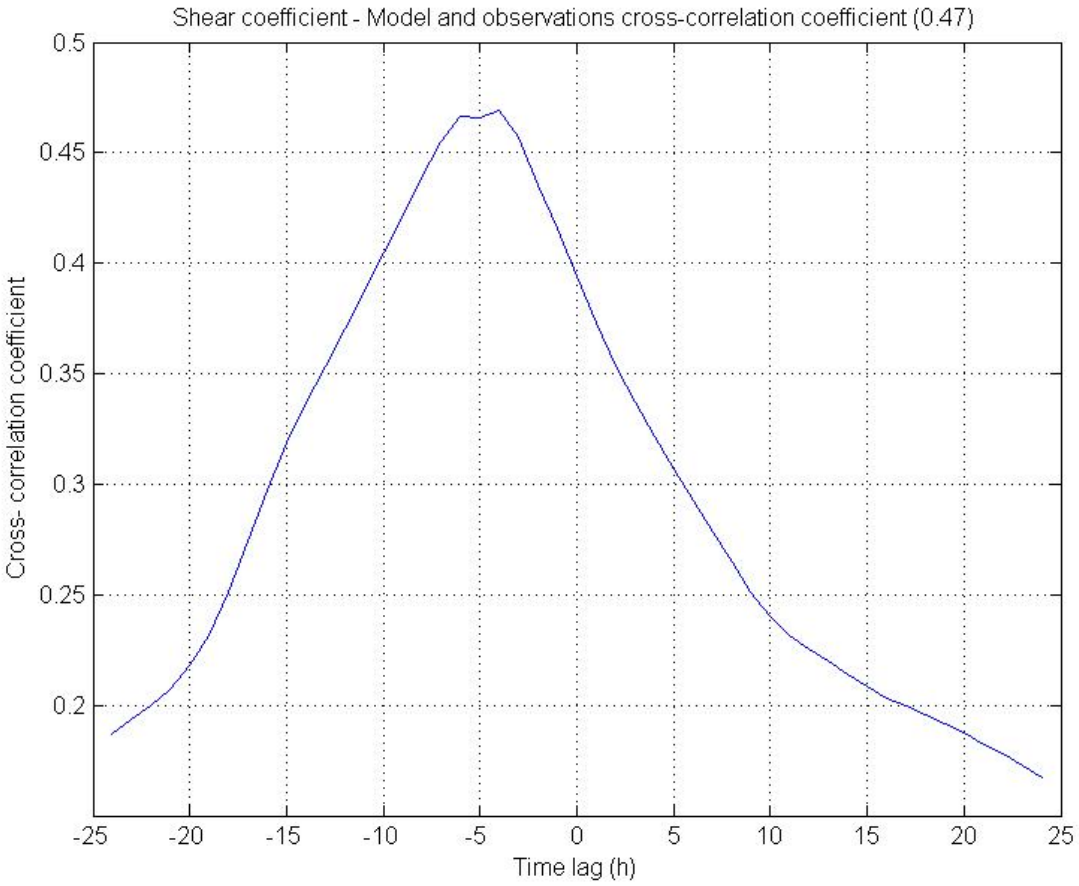

Figure 7:Cross-correlation coefficient for modeled and observed shear coefficients at Block Island AWS met Tower.

3. Spectral density

Spectral density is calculated using the Welch algorithm, using the Hanning window (to taper the time series at the beginning and end to avoid side lobe leakage). Results are shown for 31.2 m observed and simulated wind speed a s well as for power at 80 m, simulated and observed.

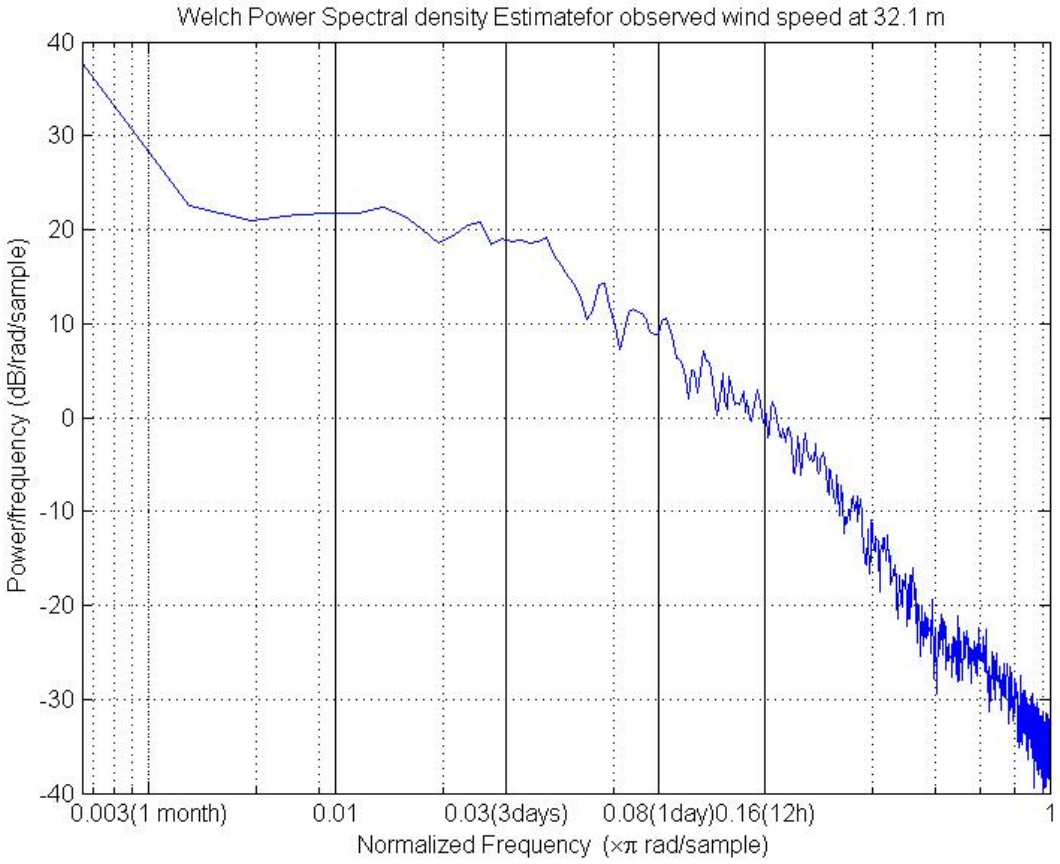

Figure 8:Welch power spectral density estimate for observed wind speeds at 32.1 m at Block Island AWS Met Tower.

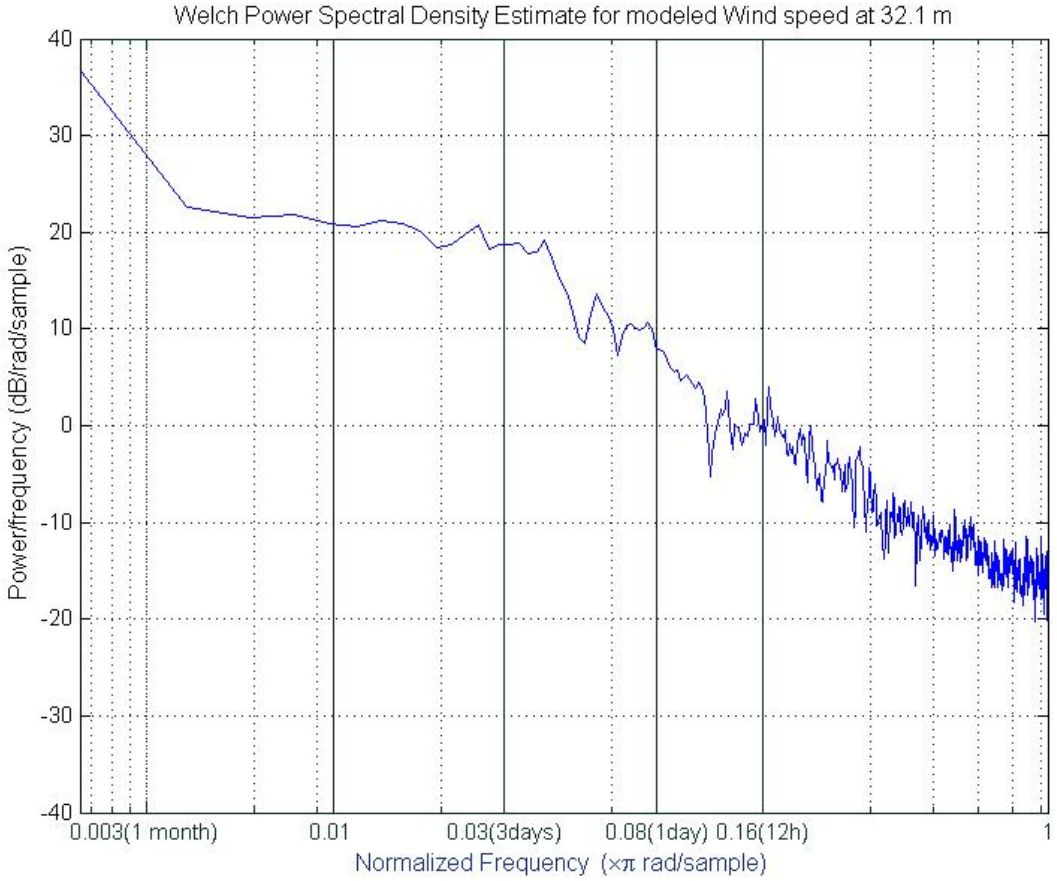

Figure 9:Welch power spectral density estimate for modeled wind speeds at 32.1 m at Block Island AWS Met Tower.

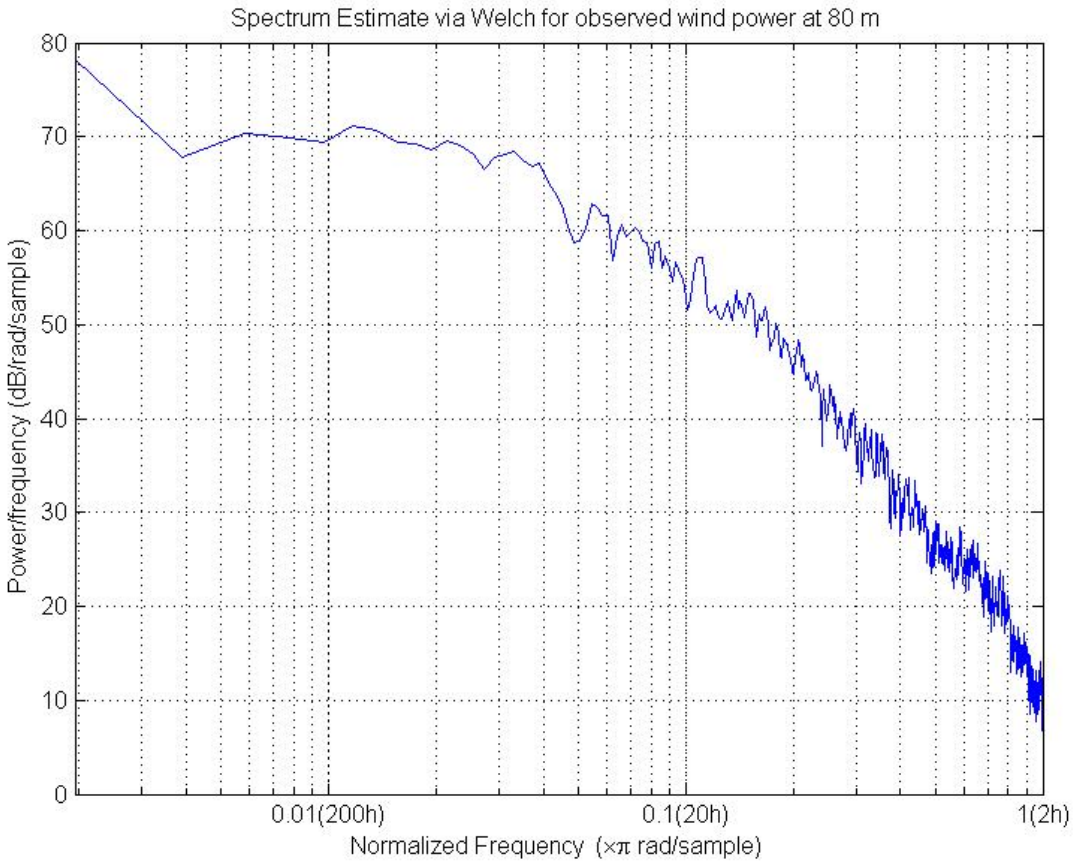

Figure 10: Welch power spectral density estimate for observed wind powers at 80 m at Block Island AWS Met Tower.

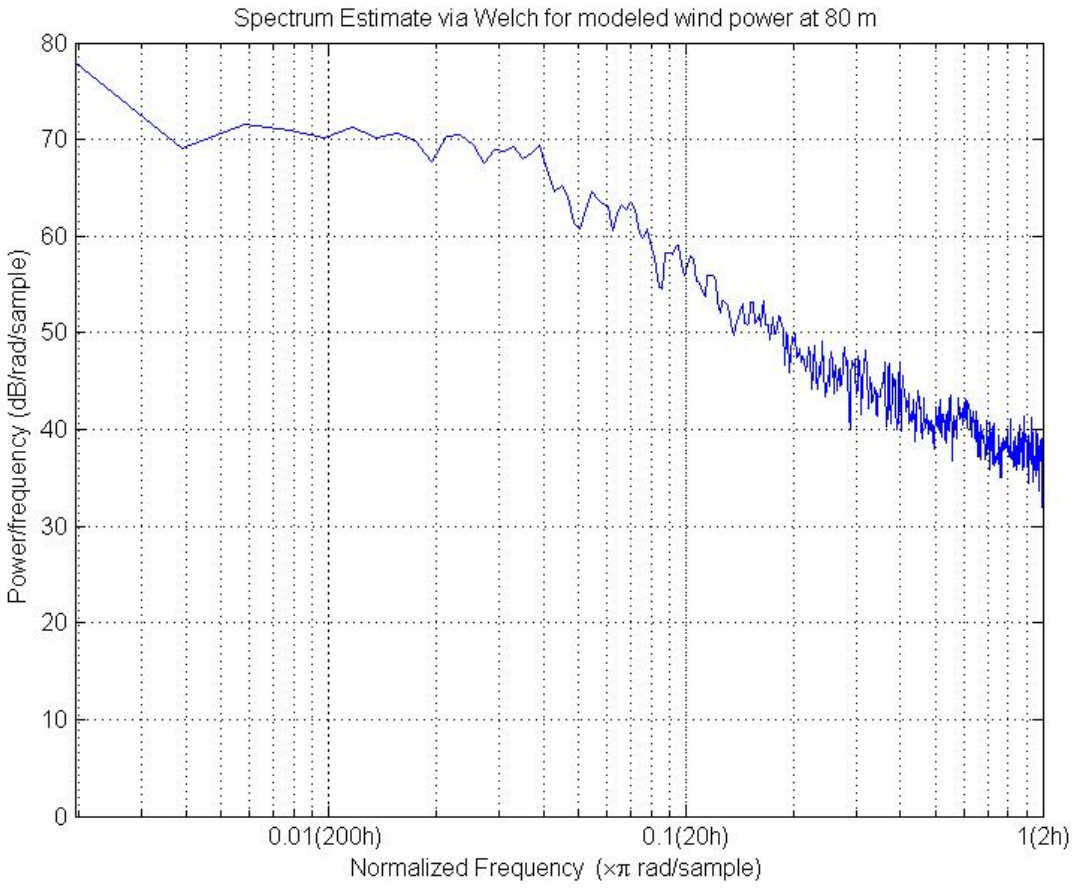

Figure 11: Welch power spectral density estimate for modeled wind powers at 80 m at Block Island AWS Met Tower.

4. Coherence

Definition

The coherence function between two stationary records x(t) and y(t) is defined as:

$$\gamma^2(f) = \frac{|G_{xy}(f)|^2}{G_{xx}(f)G_{yy}(f)}$$

where $G_{xx}(f)$ and $G_{yy}(f)$ are the estimated autospectral density function of x(t) and y(t) respectively, and $G_{xy}(f)$ is the estimated cross-spectral density function between x(t) and y(t).

The coherence function can be interpreted as the fractional portion of the mean square value of record#2 (y=simulations) that is consistent with record#1 (x=observations) at frequency f.

Results are shown for simulations (y) and observations(x) pairs, for wind speed at 32.1 m and power at 80 m in Figure 12 and Figure 13. In both cases a high coherence between observations and simulations is obtained for low frequencies up to 3 to 2 days. Then the coherence drops to be minimum for frequencies of the order of hours.

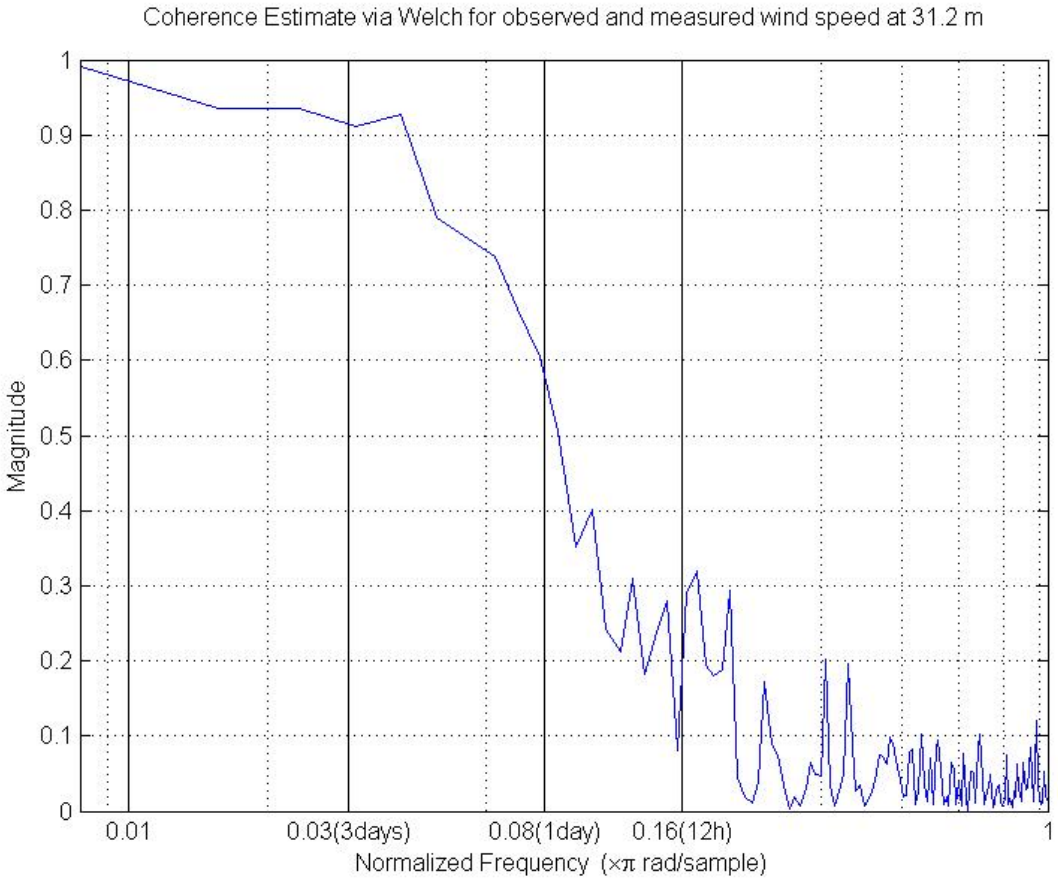

Figure 12 : Coherence estimate via Welch method for observed and measured wind speed at 32.1 m at Block Island AWS Met Tower.

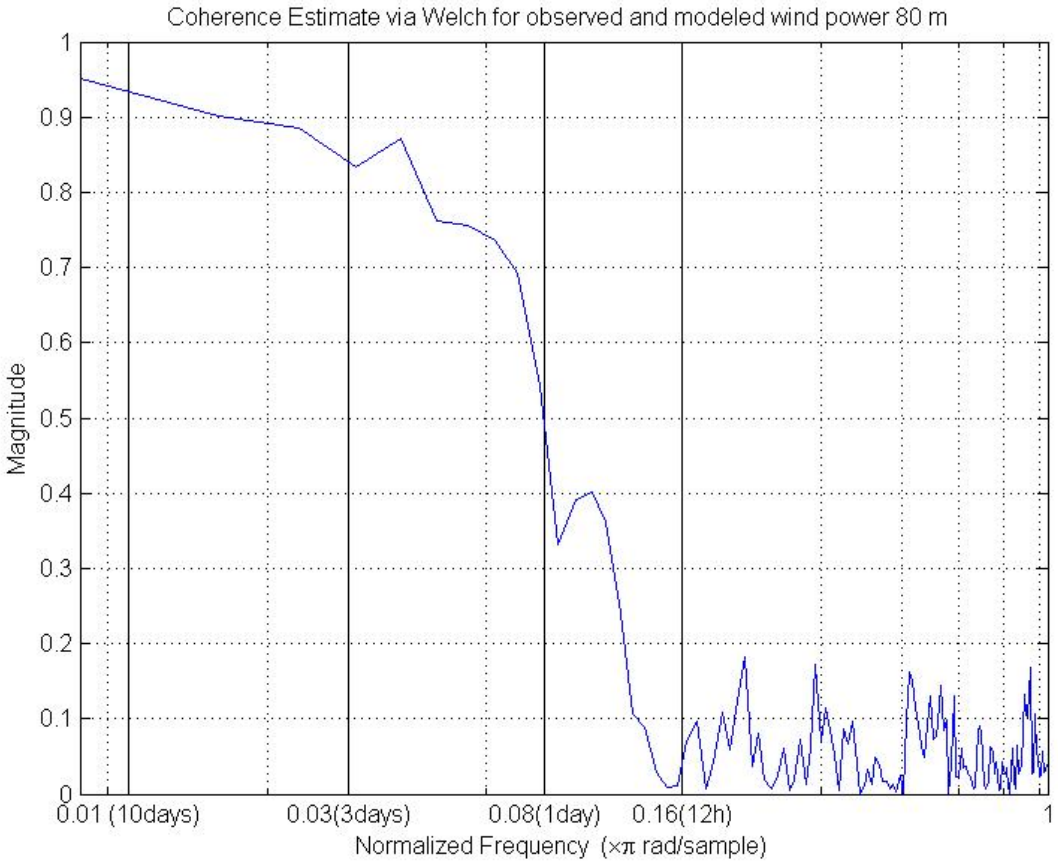

Figure 13: Coherence estimate via Welch method for observed and measured wind power at 80 m at Block Island AWS Met Tower.

5. Weibull

Time series were both fit with a Weibull adjustment (RMSE 0.2% for the modeled time series, 0.5% for the observed time series). Those adjustments are both significantly different in term of scale and shape parameters for observed and modeled time series. Values of those parameters and their confidence interval are indicated on Figure 14 and Figure 15 . However despites those discrepancies both Weibull distributions lead to very similar values of expected average power, 978 W/m^2 versus 929 W/m^2 for the observed and simulated records respectively, which correspond to a power underestimation of the model of 5% versus observations. Let's note that the simulated rose power is similarly noticeably different from the observed rose power, but both again when integrated lead to a similar power: 983 W/m^2 versus 940 W/m^2 for the observed and simulated records respectively, corresponding to a power underestimation of the model of

4% versus observations. Both methods of power estimation are in agreement with a discrepancy of the order of 0.5% for the observed record and of the order of 1% for the simulated record.

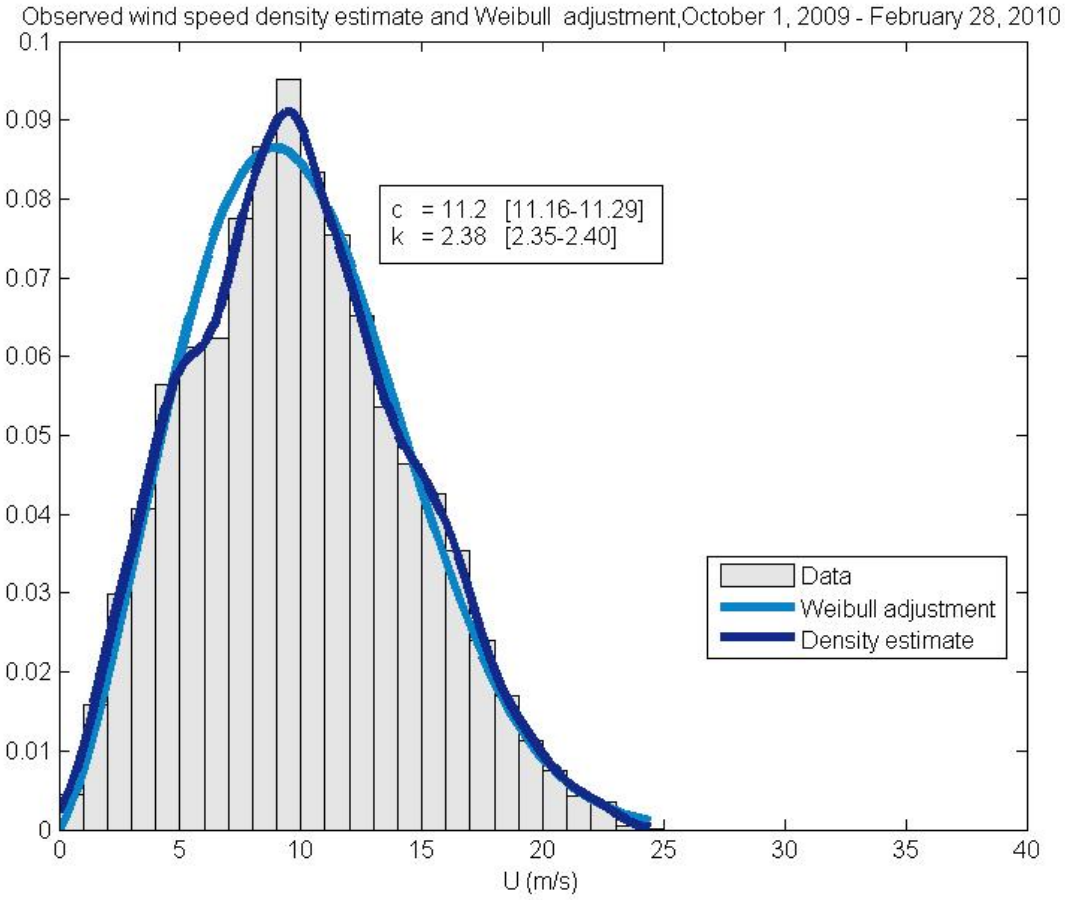

Figure 14: Weibull adjustment of observed wind speeds at 80 m at Block Island AWS Met tower.

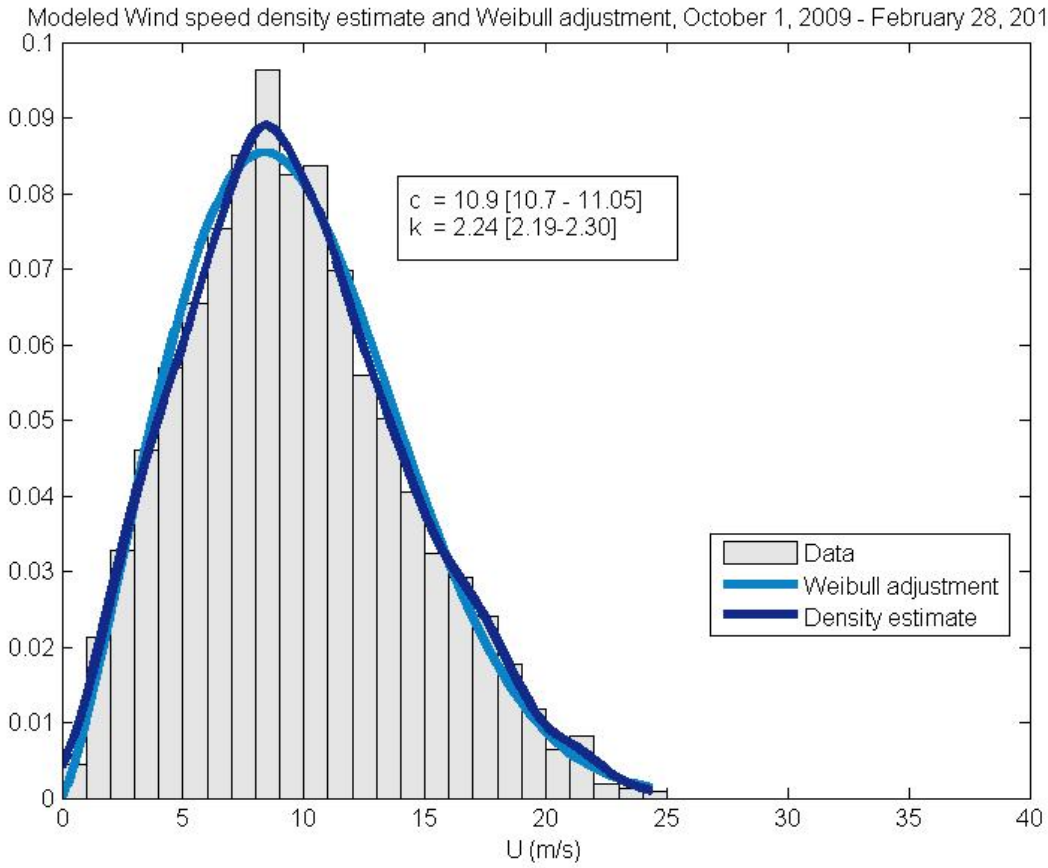

Figure 15: Weibull adjustment of modeled wind speeds at 80 m at Block Island AWS Met tower.

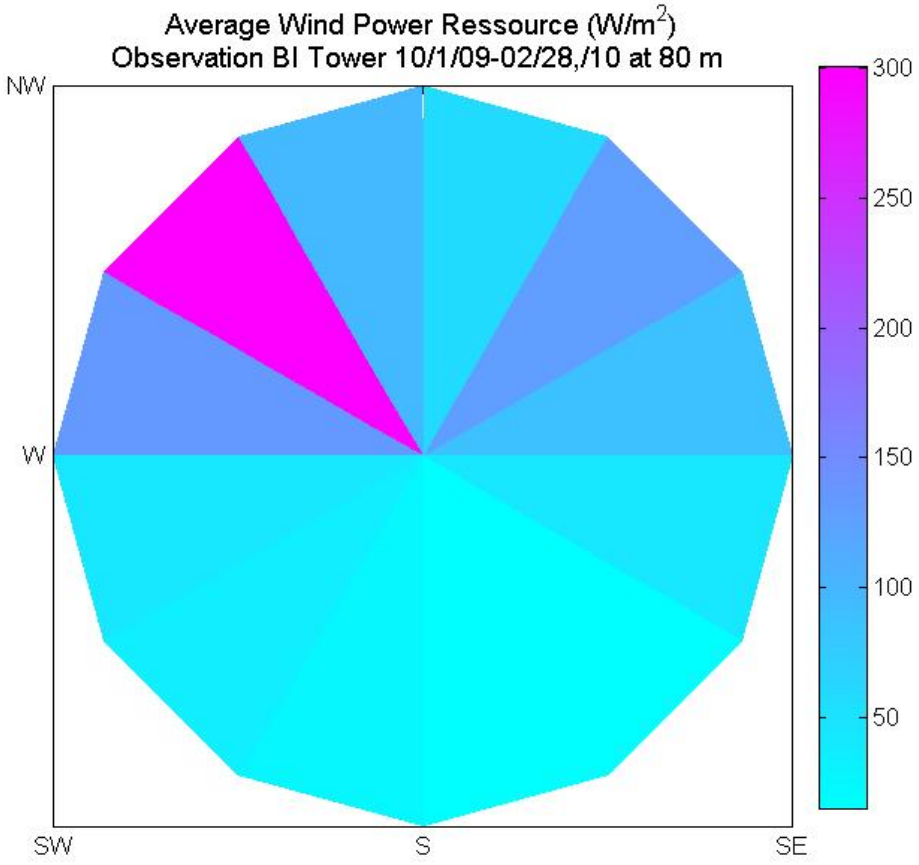

Figure 16: Average wind power resource at 80 m per directional sector estimated from time series of observations at Block island AWS Met Tower between 10/1/09-02/28/10.

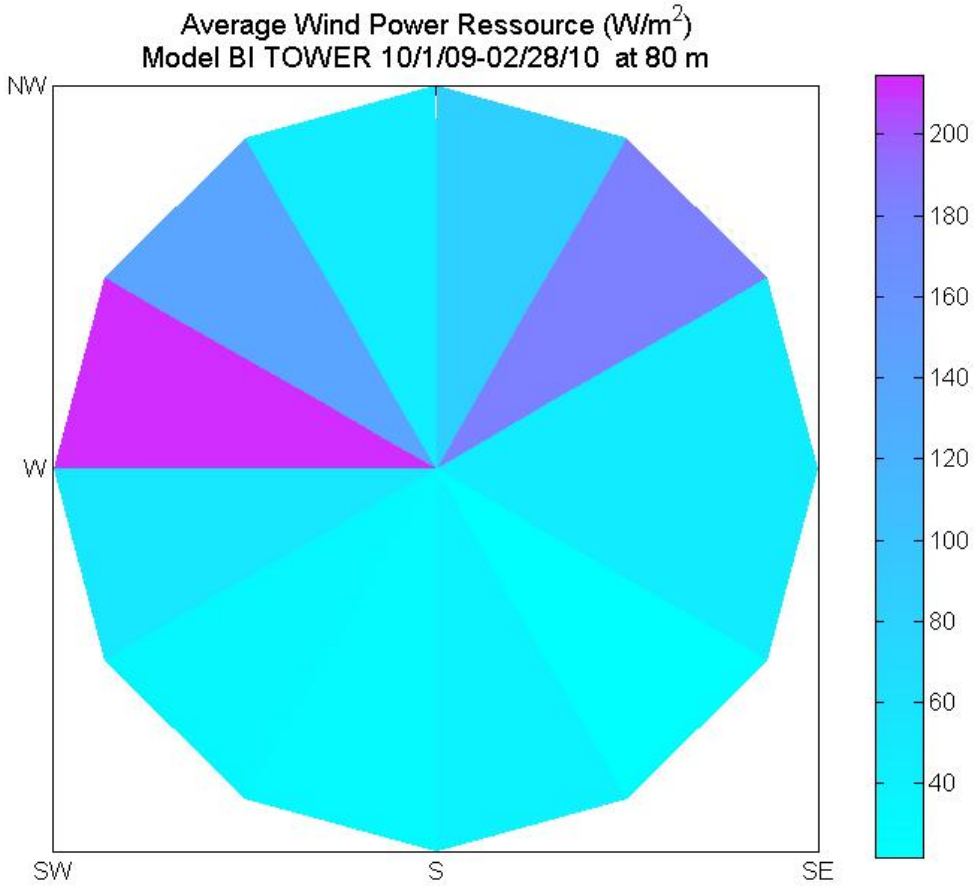

Figure 17:Average wind power resource at 80 m per directional sector estimated from time series of WeatherFlow modeled power at Block island AWS Met Tower between 10/1/09-02/28/10.